東京大学 大学院新領域創成科学研究科
基盤科学研究系
先端エネルギー工学専攻

平成 26 年度

修士論文

Taper-Tube Concentrator of Millimeter-Wave Beam for Microwave Rocket

― マイクロ波ロケットの テーパー管型ミリ波ビームコンセントレーター ―

2015 年 2 月提出
指導教員　小紫　公也　教授

47136048　Nat　Wongsuryrat

Acknowledgements

I would like to convey my sincere appreciation and gratitude to Professor Kimiya Komurasaki. For the whole 3 years includes being a research student and doing Master Degree's, owing to his valuable advice and encouragements, I could have gained many experiences, done many experiments and had many fruitful discussions with him. With his helps, I could have achieved and be proud for what I have done today.

I'm also delight to thank you to Associate Professor Hiroyuki Koizumi for his advice.

I'm grateful to Assistant Professor Tony Schonherr for much great advice and for proposed comfortable atmosphere in our laboratory during my time.

I'm also grateful to Dr.Keishi Sakamoto, Dr.Yasuhisa Oda, Dr.Ryosuke Ikeda, Dr.Ken Kajiwara and Dr.Koji Takahashi (Plasma Heating Laboratory, Naka Fusion Research Center, JAEA) for an invaluable opportunity indoing experiments at JAEA.

I obliged to all of members in Microwave Rocket's group, Mr.Toshikazu Yamaguchi, Mr.Masafumi Fukunari, Mr.Kenta Asai, Mr.Satoshi Kurita, and Mr.Yusuke Nakamura for all advice, helps and discussions. I also want to thank you all members in Komurasaki – Koizumi laboratory for giving me comfortable and enjoyable moments in Japan.

Last but not least, I would like to express my appreciation and say "thank you" to my family who has been given me infinite support.

Contents

List of Figures

List of Tables

Nomenclature

D_{e}	Taper-tube exit diameter
D_{i}	Tapered inlet diameter
E	Electrical field
Err	Error between experimental and simulation result
G_{H}	Horn antenna gain
G_{S}	Slot antenna gain
j	Imaginary unit
k	Wave number
P	Power fraction
P_{R}	Received power
P_{T}	Transmitted power
R(z):	Radius of curvature
r:	Radial distance from center axis of the Gaussian beam
S	Power Density
S_0	Peak power density
T_{L}	Taper-tube length
$U_{ionization}$	Ionization front propagation velocity
V	Voltage
x	X-axis
y	Y-axis
z	Axial distance from beam narrowest point
η_{att}	Attenuation factor
η_{trans}	Transmission efficiency
η(z):	Phase shift
θ_{ref}	Angle of reflection
θ_{t}	Tapered angle
λ:	Wavelength
ω(z):	Beam radius

Chapter 1: Introduction

1.1 Beamed Energy Propulsion

Due to the drastically increases in fossil fuel price in the latest decades, the number of rocket launched has been decreased. Future space missions, on the other hand, are still necessary to be operated in order to serve valuable purposes despite the launch cost issue. As a result, the low cost accesses to space along with the vehicle development utilizing different kind of energy source are substantially required.

Chemical rocket engines have been used since the beginning of the first rocket that entered space and has not yet changed. However, it requires the huge amount of fuel or propellant in order to launch from ground to orbit and hence its payload ratio, the mass ratio between the satellites, space probes or spacecraft carrying human or cargo over the total mass at its initial launch state which comprise of everything including the vehicle structure and fuel mass, is considerably low. This results in the extremely expensive launch cost of the rocket.

The Beamed Energy Propulsion, also known as BEP, has been proposed as one of the low cost launcher candidates having high potential in carrying sufficient payload to the orbit. Since it is expected to utilize the ground-based energy source to transmit the

energy to the vehicle, and by all means generates thrust to the vehicle. Figure 1.1 shows the illustration of BEP.

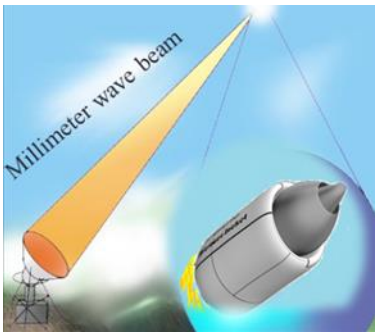

Yamaguchi et al., 2009

Figure 1.1: Illustration of Beamed Energy Propulsion. Ground-based energy source transmits energy e.g. millimeter wave, to the vehicle.

Its concept was first introduced in 1972 by Arthur Kantrowitz, using ground-based laser as a propulsion system to launch the vehicle to orbit [1]. Energy is generated on the ground-based facility and it is transmitted on to the vehicle using the specific transmission system. The transmitted energy is then conversed into propulsion energy on the vehicle. Accordingly, on board fuel is not needed to be equipped on the launched vehicle as well as turbo pump and other complicated systems are not necessary for the thrust generation. Hence, as a comparison with the conventional launching system and vehicle, BEP is expected to acquire higher payload ratio. In addition, as energy source is expected to be used on the ground, the maintenance cost is substantially low, and with the ground-based facility it could be used as many times as the vehicles are launched. Thus, the operation cost per number of vehicle launched is

considerably low as the launched count increases.

There are several numbers of researches which attempted to use laser beam as a BEP energy source and in 2001, Myrabo [2], conducted the experiment using laser and achieved the world record flights as of 71m launched.

In the thesis, on the other hand, the development of BEP's application using millimeter wave's technology as energy source so called Microwave Rocket was studied.

1.2 Millimeter Wave Technology

The frequency range of millimeter wave is from 30 GHz to 300 GHz which corresponds to wavelength of 1cm to 1mm. It is also regarded as a part of Microwave region, 0.3 GHz to 300 GHz.

A high power beam generator is required to deliver the vehicle to low earth orbits. Decades ago, such a high power beam generator was not exist, however recently the development of MW-class millimeter wave generator as known as gyrotron is achieved and showing a promising performance to be utilized as BEP energy source [3].

1.3 Concept of Microwave Rocket

Few decades ago, BEP using microwave beam as a propulsion system was started, since 1980s, the analysis on microwave rocket system was conducted [4].

Parkin et al. also proposed the concept of microwave thermal rocket using high power microwave to heat a propellant in the dielectric exchanger tube and then the heated propellant is exhausted through nozzle as in conventional chemical rocket [5], [6].

1.3.1 Microwave Rocket's Engine Cycle

The microwave rocket's model proposed by the University of Tokyo [7], [8] was studied in this thesis. The repetitive pulse millimeter wave beaming from MW-class gyrotron developed by Japan Atomic Energy Agency is expected to be utilized as energy source. Transmitted wave beam is delivered through the vehicle which it is called thruster. Pulsed plasma is then produced inside the thruster and the exhausted shockwave acquires an impulsive thrust force. This thrust generation concept has been utilized widely and also known as Pulsed Detonation Engine or PDE [9]. The advantages of this system are the simplicity of its design, and the expectation to achieve high payload ration because a thruster tube consists of only a focusing reflector and the propellant needed during its atmospheric flight is only atmospheric air. Figure 1.2 shows the schematic of Microwave Rocket which is explained as following. Thrust generation is acquired by its engine cycle starts with the process called plasma ignition where the millimeter wave beam is transmitted from gyrotron and passes through the open-end of the thruster. A focusing reflector parabolic shape, so called collector, inside

the thruster is attached at the closed-end where the millimeter wave beam is reflected and focused. Atmospheric air breakdown is occurred and plasma glows while continuously absorbing the transmitted electromagnetic wave, oscillated millimeter wave from gyrotron. Ionization front propagates towards the wave source i.e. open-end direction. Shockwave is also formed at the front of propagated ionization front of plasma and creates the pressure increment as shown in figure 1.3, pressure history of Microwave Rocket. Similarly to PDE, this is where thrust is generated. And after shockwave reaches open-end, expansion wave propagates from the exit to the thruster and pressure decreases to atmospheric pressure. Air breathing process occurs following the previous step as air inside the thruster is depressurized thus atmospheric air outside then flows into the thruster and this cycle is repeated

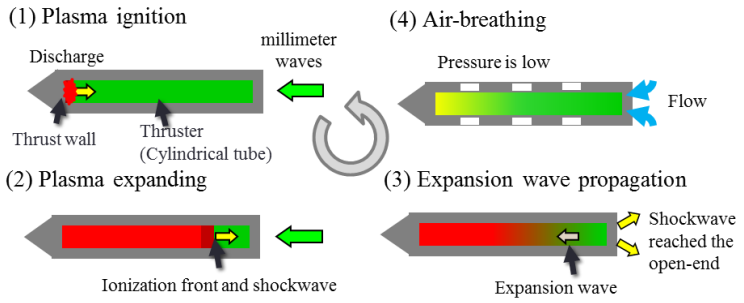

Yamaguchi et al., 2011

Figure 1.2: Engine cycle of Microwave Rocket. (1) Millimeter Wave beam is transmitted from high power source and enters the thruster. As the beam is focused by the parabolic reflector, plasma is occurred, and (2) its ionization front and shockwave propagates toward the open-end. (3) After shockwave reaches the open-end expansion wave, in contrast, propagates inside the thruster which decreases pressure inside the thruster. Thus (4) atmospheric air enters the thruster, and the cycle is repeated.

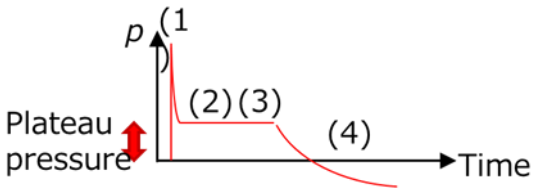

Oda et al., 2009

Figure 1.3: Pressure history inside the thruster. Numbers on the graph are 4 processes as explained in figure 1.2

1.3.2 Beam Transmission System

In this section, the high power energy source as well as the long distance transmission system is explained. In this study, on the other hand, due to the limitation of usage period of JAEA's gyrotron, a 94 GHz millimeter wave transmitter was used instead.

Gyrotron

170 GHz gyrotron is originally developed for ITER (International Thermonuclear Experimental Reactor) project [10]. JAEA has achieved steady state continuous-wave output of 1MW and the efficiency of energy conversion from electric energy to electromagnetic wave was achieved 55% [3]. Pulse length of gyrotron has been demonstrated and ranged from 0.1ms to 1000s. Its output beam mode is converted to TEM_{00} Gaussian beam by a quasi-optical mode converter and is transmitted through the corrugated waveguide to the expected experimental site. Illustration of gyrotron at JAEA and its specification shows in figure 1.4 and table 1.1 respectively.

Figure 1.4: High power millimeter wave source -Gyrotron
at Japan Atomic Energy Agency (JAEA)

Table 1.1: JAEA Gyrotron Specifications

Frequency	170 GHz
Output Power	< 1MW
Beam Profile	HE11 (Gaussian)
Beam Waist	20.4 mm
Electrical Efficiency	< 60%

Beam transmission system

Output of gyrotron is a Gaussian beam profile and its equation is shown in Eq.1.1

$$E(r,z) = E_0 \frac{\omega_0}{\omega(z)} exp[-j\big(kz - \eta(z)\big) - r^2(\frac{1}{\omega^2(z)} + \frac{jk}{2R(z)})] \qquad 1.1$$

where E is electrical field, r is radial distance from the center axis of the beam, z is the axial distance from the beam's narrowest point i.e. beam waist, 0 denotes the

position at the center of the beam, ω(z) is the radius at which the field amplitude and intensity drop to 1/e and $1/e^2$ of their axial value respectively , j is the imaginary unit, k is wave number, *R(z)* and *η(z)* denote radius of curvature and phase shift which are the relations related to z and are shown in Eq.1.2 and Eq.1.3.

$$R(z) = z[1 + \left(\frac{\pi\omega_0^2 n}{\lambda z}\right)^2] \quad 1.2$$

$$\eta(z) = arctan(\frac{\lambda z}{\pi\omega_0^2 n}) \quad 1.3$$

In addition, Gaussian beam parameters, beam spot size, Rayleigh range, and beam divergence angle (in radians) can be defined as in Eq. 1.4, 1.5 and 1.6 respectively.

$$\omega(z) = \omega_0 \sqrt{1 + (\frac{z}{z_R})^2} \quad 1.4$$

$$z_R = \frac{\pi\omega_0^2}{\lambda} \quad 1.5$$

$$\theta_d \cong \frac{\lambda}{\pi\omega_0} \quad 1.6$$

From the above equations, it certainly shows that in order to obtain well collimated beam output in a certain distance (Rayleigh length), beam waist has to be increased to suppress beam divergence angle. Figure 1.5 shows the experimental schematic using beam transmission system to expand gyrotron output's beam waist [11]. This transmission system gives Rayleigh length approximately 26 meters.

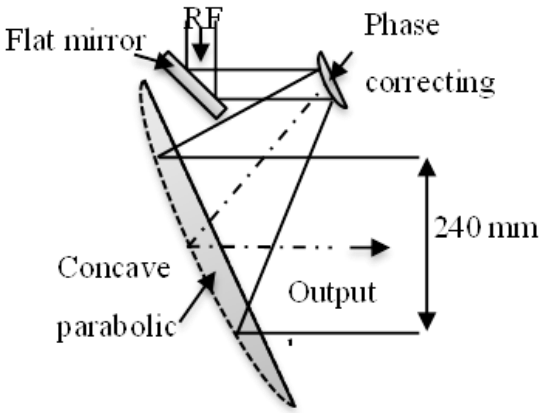

Fukunari et al., 2013

Figure 1.5a: Beam transmission system, creating collimated beam. 170 GHz Gyrotron transmits high energy millimeter wave beam passes through corrugated waveguide. Flat mirror collects the beam at the waveguide exit and reflects the entire beam to phase correcting mirror and then parabolic mirror. Resulting in expanding 20.4mm beam waist to 120 mm, which gives Rayleigh length approximately 26 m.

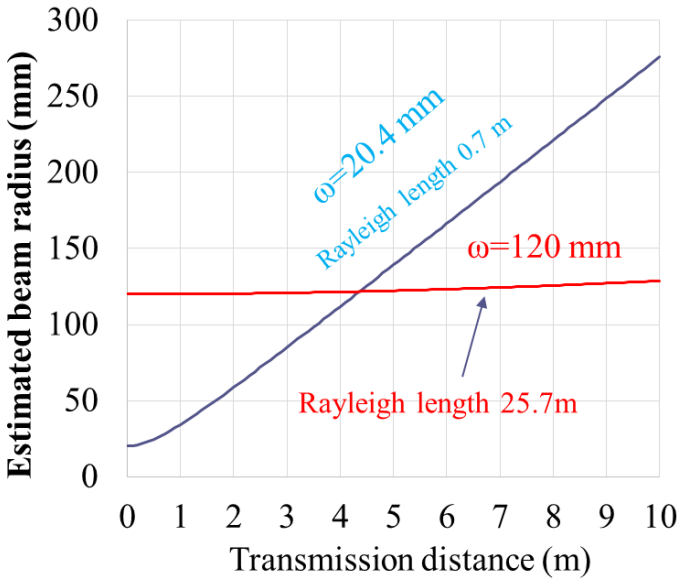

Figure 1.5b: Relation between transmission distance (x-axis) and estimated beam radius (y-axis) at 20.4 mm and 120 mm. This graph shows that with the beam transmission mirror system, beam is collimated with Rayleigh length equals to 25.7 m.

Beam receiving system

Figure 1.6 illustrates the long distance launch experimental schematic, and it is explained as the following. Incident beam is generated by gyrotron through corrugated waveguide and it is reflected the beam transmission system in order to create expanded-collimated Gaussian beam. Thus, before the transmitted beam enters thruster, beam receiving system is necessary to collect the beam and to guide it into the thruster. For simplicity, it was designed as taper waveguide with the large-end receiving the incident beam while the small diameter side is used to connect with the thruster. Nonetheless, previous research [12] also shows that different incident beam profile before it enters thruster, which could be altered by beam receiving system, has an effect on thrust generation. Figure 1.7 and table 1.2 shows the effect of beam profile to thrust generation.

Resulting in, the development and investigation of taper-tube beam concentrator as Microwave Rocket beam receiving system.

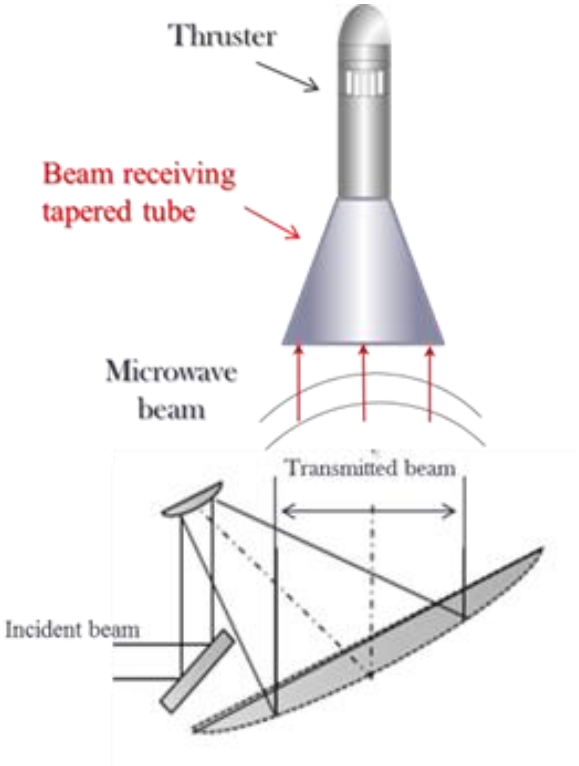

Fukunari et al., 2013

Figure 1.6: Microwave Rocket long distances launch experiment schematic. Transmitted beam is expanded using beam transmission system. Beam receiving taper-tube concentrator is designed to collect the expanded beam and guides it into the thruster.

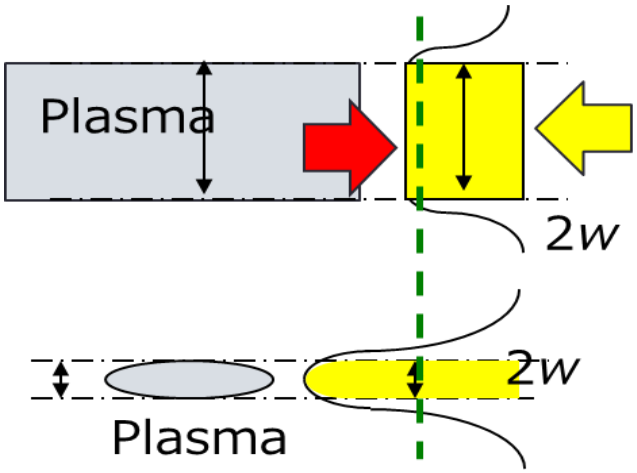

Yamaguchi ei al., 2011

Figure 1.7: Illustration of plasma shape inside the thruster due to different beam profile, flat-top (above) and Gaussian (below)

Table 1.2: Effect of beam profile to thrust impulse

Properties	Gaussian	Flat-top
Peak power density	33 kW/cm2	16 kW/cm2
Ionization front propagation velocity	140 m/s	68 m/s
Thrust impulse	13.2 mNs	28.4 mNs

Yamaguchi et al.,2011

1.4 Low Power Facility – 94 GHz Transmitter

Since it is not possible to conduct the experiment using gyrotron as many times as it is expected, in this study 94GHz oscillator manufactured by ELVA-1 was used as beam source instead. It capable of transmit millimeter wave with power approximately 400mW.

Transmitter was attached with horn antenna and generated millimeter wave reflected the parabolic mirror to collimate the beam in a similar manner as explained earlier in beam transmission system section. Receiver equipped with slot antenna was located in the far field facing the parabolic mirror, and it is used to detect the incident beam. Experimental and measurement apparatus is explained in details in the following chapter. Figure 1.8 shows 94GHz oscillator and its receiver.

Figure 1.8: 94 GHz Transmitter (right), receiver (left), and their power supply.

1.5 Ray Tracing Method

To design Microwave Rocket's taper-tube concentrator, ray tracing method was used. FDTD was widely used [13] in electromagnetic wave field in designing and simulating interesting subject however, in this study, considering the size of taper-tube being used ray tracing method was computed instead due it its simplicity and low computation cost. Since wavelength of millimeter wave transmitted by 170GHz gyrotron is very much smaller compare to the receiving taper-tube concentrator size as well as the Microwave Rocket thruster, hence transmitted millimeter wave is expected having behavior similar to ray of light. So that ray tracing was chosen. Assuming that wave behaves similar to the ray of light, it neglects all wave effects and considers each ray as an importance matter instead. The method which is so called Ray Tracing thus was used to simulate the wave propagation inside the receiving taper-tube concentrator. This method is also widely used in many millimeter wave applications [14], [15].

Moreover, it is interesting to note that tapered waveguide has been studied for

several decades [16], [17] however its size was usually small compare to the taper-tube in this study. As the applications being used are difference, the challenge of this study is to examine the taper-tube concentrator of millimeter wave for Microwave Rocket through experiment as well as simulation.

1.6 Objectives

Thrust performance of Microwave Rocket also relies on the transmission efficiency of the beam receiving system as it is expected to deliver the entire incident beam to the thruster. By using the Ray Tracing method and 94GHz oscillator for the experiment it is expected that even though the simulation method doesn't taken into account of wave effects it could reproduce the experimental results.

As a result, this study aims to

(1) To identify the transmission efficiency of the taper-tube concentrator using 94GHz transmitter and receiver from the measurement

(2) To show the consistence between the simulation and experimental results that ray tracing method is applicable for Microwave Rocket's taper-tube design.

(3) To investigate the ionization front propagation velocity inside Microwave Rocket equipped with taper-tube concentrator using Gyrotron.

Chapter 2: Millimeter Wave Transmission Experiment

2.1 Experimental Equipment

As mentioned earlier, 94GHz oscillator was used instead of gyrotron in order to investigate transmission efficiency of taper-tube concentrator and the beam profile at its exit. Hence to prove that, in this section, experimental and measurement equipment is explained.

2.1.1 Transmitter and Receiver

The transmitter and receiver used in the experiment shown in figure 1.7 in the previous chapter are Tx/Rx modules W-band 94GHz Model TR-10/94/x**,** were manufactured by ELVA-1 Company. Its provided specification is shown in table 2.1 and figure 2.1 shows block diagram of the system.

Table 2.1: 94GHz transmitter and receiver specifications

Parameters	Specified	Measured
Transmit Frequency	94.99 GHz	94.99 GHz
Transmit power	400 mW	415 mW
Noise figure Rx	8 dB	6.8 dB
Variable attenuator	0-30 dB	0-40 dB
Video output bandwidth	DC – 5MHz	DC – 5MHz
Waveguide connectors	WR-10/UG-387/U-M	WR-10/UG-387/U-M
Video IQ outputs	BNC	BNC
Operating Temperature		+10 to +40 deg. C

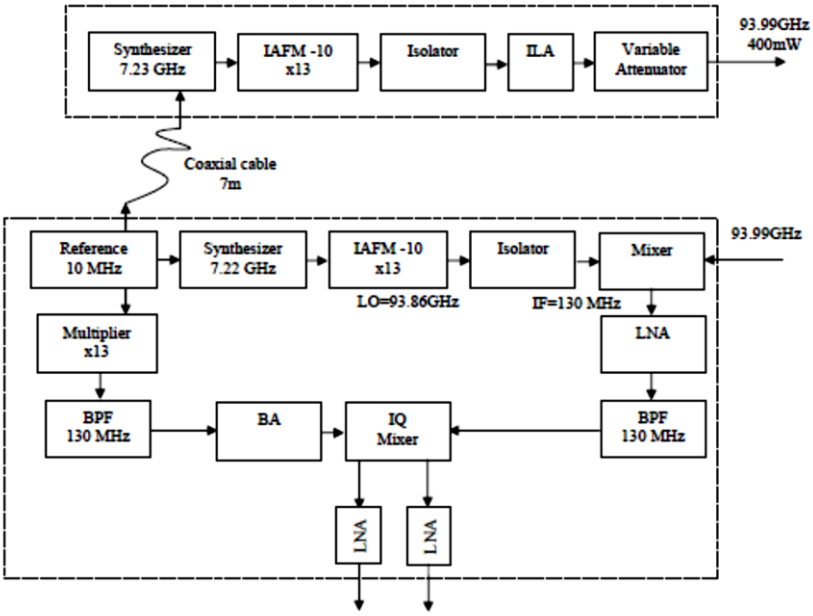

Figure 2.1: Block diagram of Tx/Rx system

Horn antenna, manufactured by Millimeter Wave Products Inc., was connected with the waveguide output of the transmitter to oscillate the 94GHz millimeter wave. Its geometry and specification, as well as its radiation pattern are shown in figure 2.2, and 2.3 respectively. Meanwhile, receiver was equipped with slot antenna for 94GHz from the same manufacture with length 50mm.

2.1.2 Collimate mirror

Eq. 2.1 shows the formula of the parabolic mirror that was used to collimate the divergence millimeter wave from horn antenna. Its focal length is equal to 278.99mm. This mirror was designed earlier prior to this study, on the other hand it was utilized for the purpose of collimating the beam for this study.

$$y = (8.961\text{x}10^{-4})x^2 \qquad 2.1$$

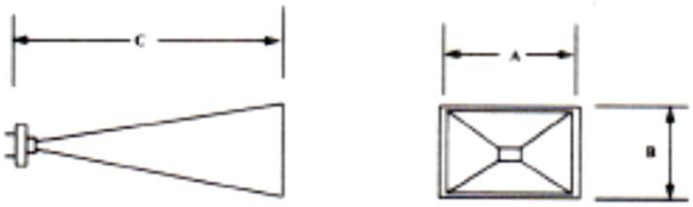

Millimeter Wave Products Inc

Figure 2.2: Horn antenna model 261W.
A=30.7mm, B=25.9mm, and C=71.1mm

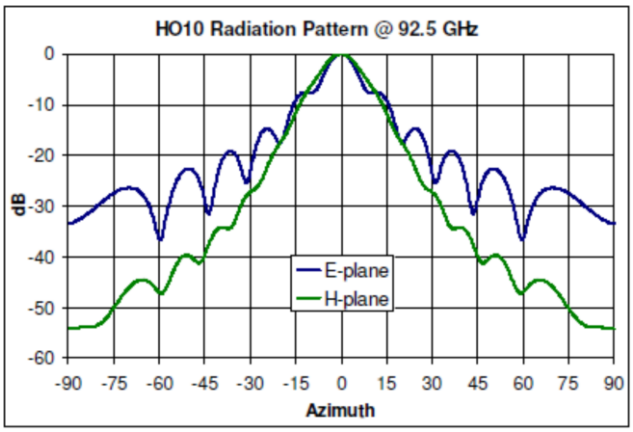

Millimeter Wave Products Inc

Figure 2.3: Horn antenna radiation pattern

2.1.3 Two Dimensional Moving Stages

Receiver was fixed on two dimensional moving stages when it was used to measure the millimeter wave on the far field. Two-Axis Stage GSC-02 controller was connected with the Translation Motorized Stages SGSP26 series, manufactured by Sigmakoki Co., Ltd., the stages were moved to the desired position by commands sent from the PC through the controller. Maximum length for both horizontal (*x*-axis) and vertical (*y*-axis) is 200 mm.

2.2 Experimental Setup and Analysis Method

2.2.1 Millimeter Wave Beam Transmitter/Receiver and Alignment Setup

The 94GHz transmitter was setup on the custom made adjustable stage, and height as well as tilt angle with respect to the ground can be adjusted. It was located facing the parabolic collimate mirror at the distance equals to its focal length. Mirror was fixed with tilt stage so that tilt angle is accurately adjusted.

Receiver was fixed on the two dimensional moving stages on the far field from the collimate mirror. It is critical to ensure that the slot antenna used with the receiver has zero or at least minimum tilt angle with respect to the collimated beam from the mirror so that the effect of antenna gain is minimized. Thus, planar laser was deployed to accurately adjust the beam alignment.

The setup is explained as following, first planar laser was pointed to the collimator mirror and it reflected the laser beam back to the focal point in which horn antenna was located. On the other hand, in an opposite direction – 180 degree turns around, planar laser was fixed on the aluminum supportive rod and along this aluminum rod, it was considered as fixing line (beam direction). This rod was represented as the invisible collimated beam direction and it was used along with the laser to locate position of the receiver at the far end. Figure 2.4 shows the explained experimental

setup. ECCOSORB: High Loss Absorbers were deployed at the experimental area to prevent any undesired reflection if any.

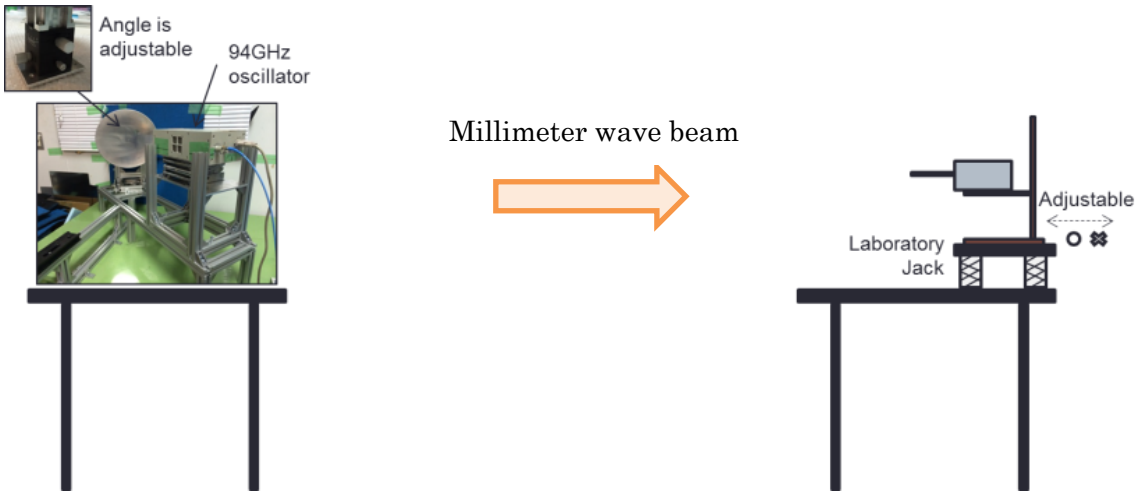

Figure 2.4: Illustration of experimental setup. 94GHz transmitter is fixed on adjustable height custom made stage. Collimate mirror is fixed with tilt stage. On the other hand, receiver is fixed on two dimensional moving stages on the far field.

2.2.2 Calibration Data

Receiver was connected with the voltage doubler rectifier circuit to obtain the stable output signal read by oscilloscope and PC. Since the measured values of experimental results would contain errors from electrical losses or either from connections between devices as well as the read voltage was doubled for the purpose of measurement, if it's too low then PC always read as zero. Thus some calibration data is required.

As mentioned, receiver was connected to PC, however the results shown in PC was actually slightly difference from the actual value measured by oscilloscope. Hence,

prior to the actual experiment, calibration curve between actual voltage and displayed voltage on PC was conducted. Figure 2.5 shows the circuit calibration data in which x-axis represents the voltage PC displays, $V_{\text{out,}}$ while y-axis represents actual voltage, V_{in}. The circle plots on the graph represent the experimental value, and fitting lines were made for approximation.

Furthermore, the estimation of actual power was taken into account of losses in free space. Eq.2.2 shows electromagnetic wave free space loss relation. This equation was used coupling with actual voltage to estimate actual power measured by the receiver. Figure 2.6 shows the graph used to estimate actual power measured by receiver from voltage where *x*-axis is power in μW and *y*-axis is voltage in mV. Equation of fitting line used for the estimation is shown in Eq.2.3.

$$P_{\text{R}} = (\frac{\lambda}{4\pi r})^2 G_{\text{s}} G_h \eta_{\text{att}} P_{\text{T}} \text{ ;} \qquad 2.2$$

$$\text{V} = 1276.5\sqrt{P_{\text{R}}} \qquad 2.3$$

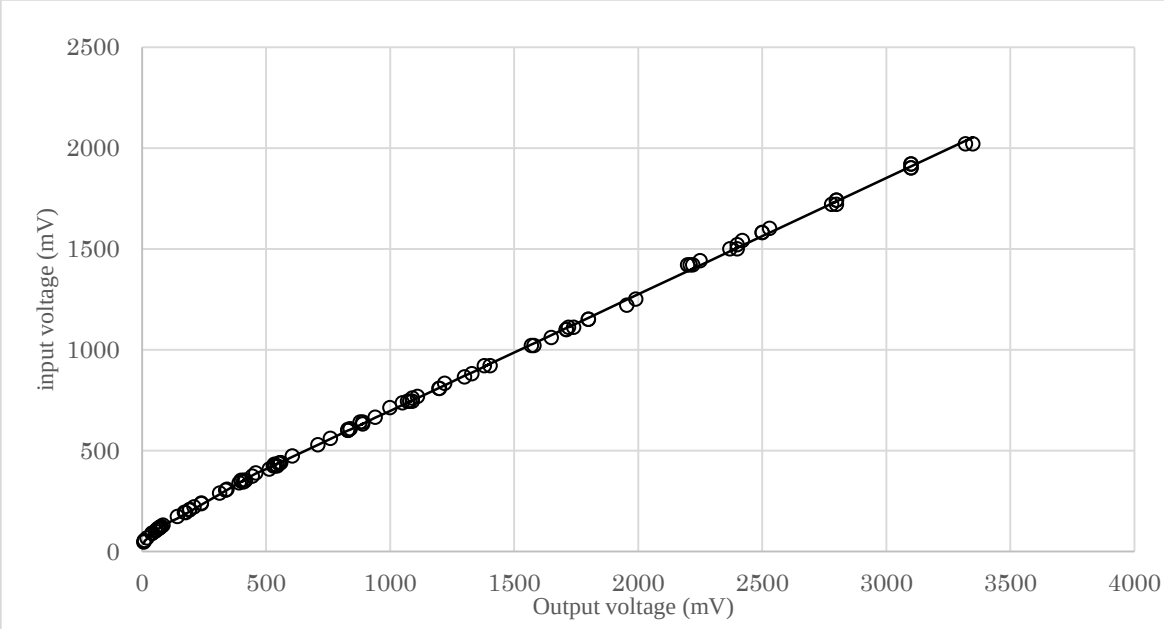

Figure 2.5: Voltage doubler rectifier circuit calibration data. X-axis and Y-axis represent detected voltage after the circuit, and actual voltage respectively.

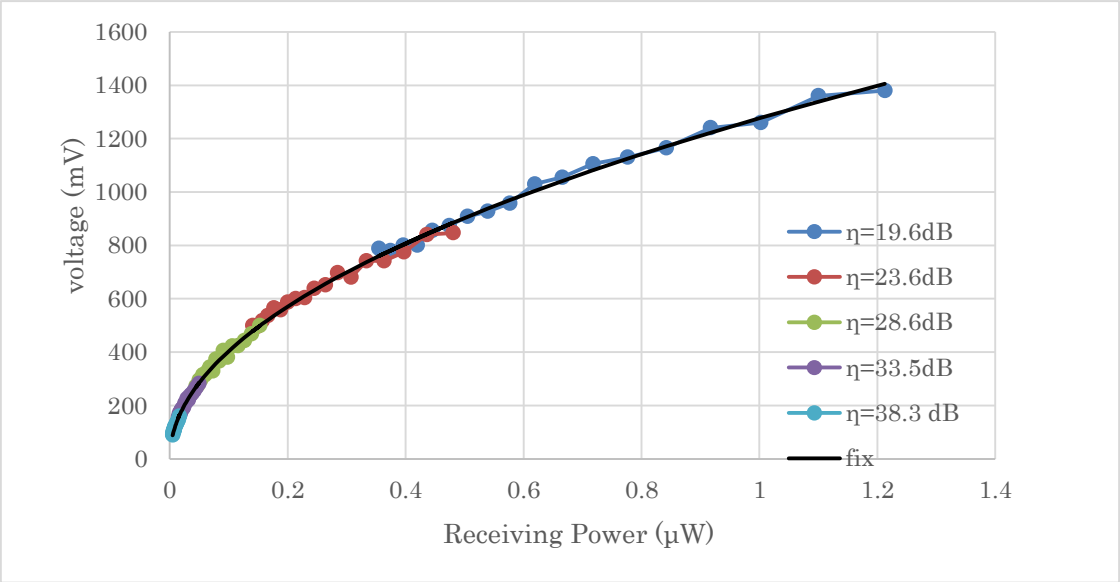

Figure 2.6: Estimation of actual receiving power. *x* and *y* axis represent receiving power in μW, and actual voltage in mV respectively.

2.3 Experimental Results and Discussion (Incident beam)

As with the experimental setup shown in figure 2.4, collimated incident beam measurement was conducted using 94GHz transmitter and receiver. Center of the beam and beam radius was estimated using momentum method, Eq.2.4a and 2.4b respectively. Result is shown in figure 2.7, and table 2.2.

$$\langle x^n \rangle = \int x^n I(x,y)dxdy \Big/ \int I(x,y)dxdy \qquad 2.4a$$

$$\omega = 2\sqrt{\langle x^2 \rangle - \langle x \rangle^2} \qquad 2.4b$$

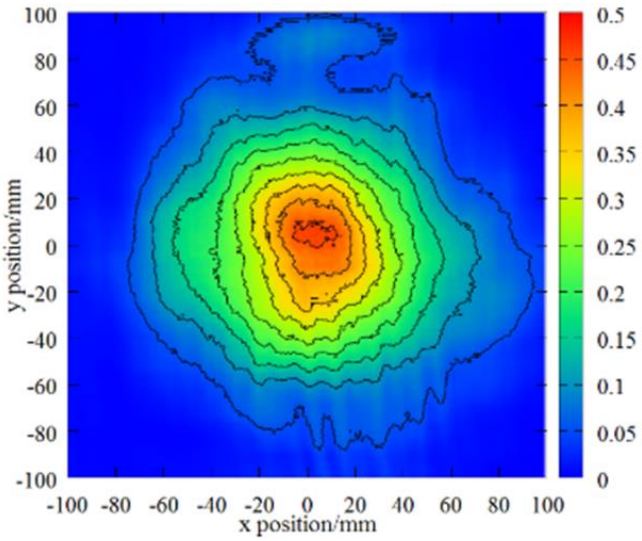

Figure 2.7: Incident beam. Transmitted wave from 94GHz transmitter was collimated by parabolic mirror and measured by the receiver. Distance from collimate mirror to the receiver was 220 mm. Measurement plane was 200 mm x 200 mm.

Table 2.2: Experimental Results (Incident beam)

Parameters	x-axis	y-axis
Center	103.9 mm	99.5 mm
Tilt Angle	0.1°	-0.013°
Beam Width	72.6 mm	75.4 mm
Total power	3.63 mW	

Results show that there are tile angles in both *x* and *y* axis but in very small degree. Thus, center of the beam was not perfectly aligned with center of measurement plane, at 100 mm in both *x* and *y* axis. Beam width in *x* and *y* axis was also slightly different. Beam profile of incident beam is similar to Gaussian profile.

The differences in center of the beam as well as beam width might occur due to the alignment error between the transmitter and collimate mirror. Several points must be taken into account for instance, transmitter was probably not perfectly placed right at the focal point of the parabolic mirror in order to create the parallel beam, and also small tilt angles were exhibit at the mirror. In the far field, on the other hand, receiver was maybe not perfectly align with the center of the mirror but slightly missed. Some interference with the surroundings also probably exhibited at the edge of the incident beam.

In addition, the integration of incident beam result was done, and it was estimated 3.63 mW. Incident beam measurement also shows that with the current transmitter, 94GHz, and the collimate mirror being used, Rayleigh length is approximately 5.5 meters which is sufficient enough for the experiments in this study in the following chapter.

2.4 Conclusion

In order to investigate the transmission efficiency of taper-tube concentrator, low power beam source - 94GHz transmitter was used. The experiment was conducted using 94 GHz transmitter equipped with horn antenna to transmit millimeter wave beam. Collimate mirror was then used to reflect entire beam and created parallel beam. Collimated beam was measured using receiver at distance 220 mm. The measurement system consisted of 94GHz receiver and two dimensional moving stages. Measurement surface area was 200 mm in both x and y axis.

The experimental result shows the incident beam profile which is similar to Gaussian beam profile. Beam width was 72.6 mm and 75.4 mm in *x* and *y* axis respectively. Center of the incident beam slightly missed from the center of measurement plane. However, there were only small tilt angle in both *x* and *y* axis, 0.1°and 0.013°respectively.

Chapter 3: Taper-tube Concentrator

3.1 Design Parameters and Variables

Ray tracing simulation method was used to design the taper-tube concentrator. This method has been used on millimeter wave researches due to its advantageous in simplicity and low computation cost. Ray tracing, however, has few of significant parts to be considered i.e. it works as tracing each injected ray to subject of interest thus millimeter wave is treated as ray of light and its wave effect is neglected.

As a result, the size of subject to be investigated has to be much large than the wavelength been used. In case of Microwave Rocket, the wavelength of millimeter wave transmitted from gyrotron is very small and approximately 1.7 mm compare to the size of taper-tube concentrator, the behavior of the wave is assumed to be similar to ray of light, thus neglect wave effects.

In this study, 94 GHz transmitter was used, and its wavelength is approximately equal to 3.2 mm which is still very small compare to the designed taper-tube. Design parameters and variables are explained as followings.

3.1.1 Parameters and Variables

There were 4 parameters and variables to be considered, (1) D_{i}, taper-tube inlet

diameter, (2) D_{e}, taper-tube exit diameter, (3) θ_{t}, tapered angle, and (4) T_L, taper-tube length. Figure 3.1 illustrates taper-tube parameters and variables.

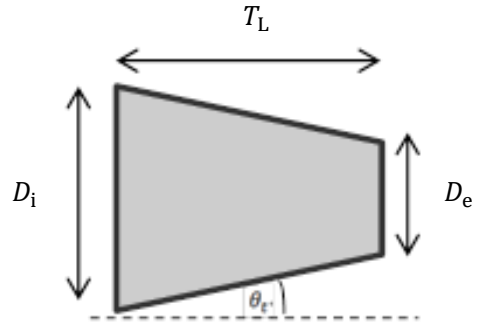

Figure 3.1: Taper-tube concentrator parameters and variables.

First thing first, taper-tube inlet diameter is varied with the incident beam diameter. Since the purpose of taper-tube concentrator is to convey the entire incident beam to the thruster, inlet diameter is supposed to be larger than the incident beam diameter. And from the experimental result in section 2.2 it is shown that the beam diameter in both *x*-axis and *y*-axis is approximately 150 mm. Hence, in this study inlet diameter of 180 mm was used. It is slightly larger than the beam diameter to ensure that entire beam is entered the taper-tube without any spill over; beam that does not enter the inlet of taper-tube.

3.1.2 Design Criteria

Figure 3.2 illustrates the ray tracing simulation on taper-tube. In the figure, it is shown that if the wave is treated as rays of light, when each ray hit with the taper-tube wall, reflection occurs. Eq.3.1 shows the angle of reflection (θ_{ref}) with respect to the

horizontal axis that depending on the number of reflection (n) inside the taper-tube. As a result, taper-tube illustrated in figure 3.2 shows 4 types of ray. First, in this study it is called (i) No reflection beam which are rays that injected into the taper-tube and don't hit any part of the taper-tube. Thus they pass through the taper-tube as straight lines align with horizontal direction. And they are shown as purple lines in figure 3.2. Blue rays in figure 3.2 were called (ii) 1-reflection beam. They hit taper-tube wall once before they leave at taper-tube exit. Green rays, on the other hand, they reflect twice and hence θ_{ref} is larger than 1-reflection beam case. They were noticed as (iii) 2-reflections beam. Red rays, (iv) backward reflection beam, they are an undesired condition as if they exist, some of the incident beam reflects back in the incident direction and that means not an entire incident beam passes through taper-tube.

As a consequence, it is important to note that to decide each values of other 3 design variables; taper-tube length, tapered angle, and taper-tube exit diameter, backward reflection must be avoided.

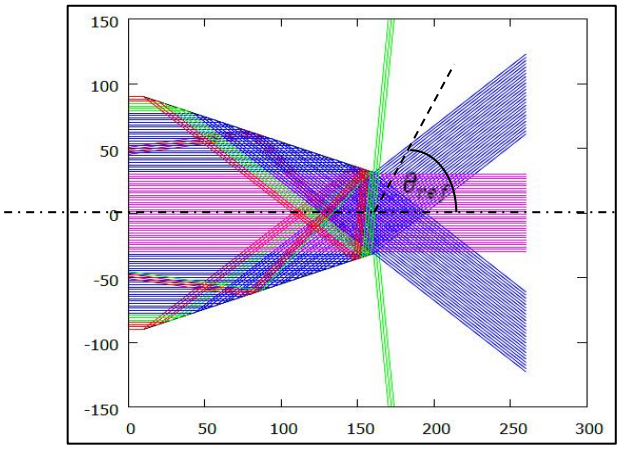

Figure 3.2: Illustration of ray tracing 2D computation result. (i) Purple/center rays were called no reflection beam as they were not reflected inside the taper-tube before they left taper-tube exit. Meanwhile, (ii) and (iii) were 1-reflection and 2-reflections beam respectively, and they are shown as blue and green rays in which 2-reflections beam leave taper-tube exit with larger θ_{ref}. (iv) backward reflection which is an undesired condition.

$$\theta_{\mathrm{ref}} = 2n\theta_{\mathrm{t}} \qquad 3.1$$

3.1.3 Design Curve

Figure 3.3 shows the design curve from ray tracing result with taper-tube inlet diameter of 180 mm. The x-axis and y-axis are taper-tube length and tapered angle respectively. Exit diameter was chosen considering that it is much larger than the wavelength being used, and it was 65 mm compare to the wavelength at 3.2 mm.

With the fixed numbers of taper-tube inlet and exit diameter, length and tapered angle was plotted. Along the curve are the usable values without any backward reflection occur. Straight lines denote the maximum reflections that occur inside the taper-tube.

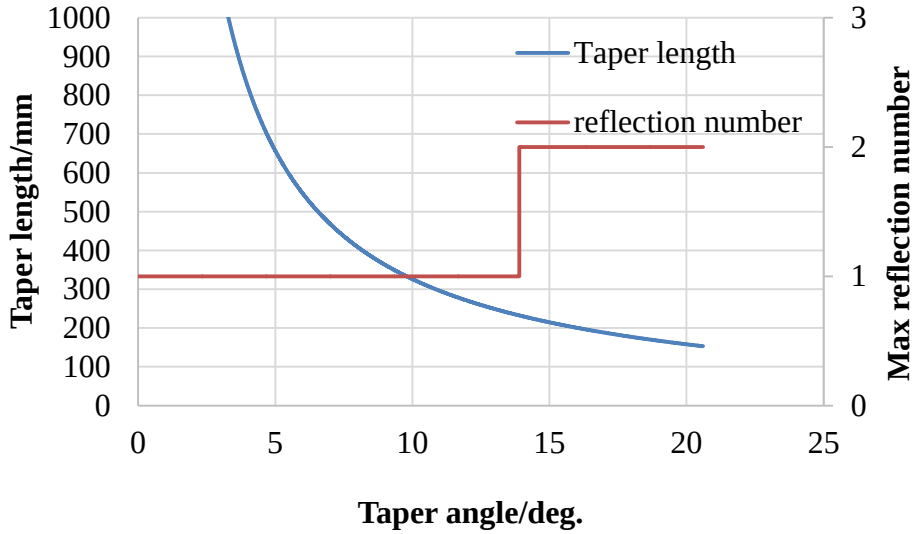

Figure 3.3: Ray tracing result on taper-tube length (x-axis) and tapered angle (y-axis). Blue curve is the plot between length and angle while orange straight lines denote maximum reflection that occurred inside taper-tube..

As a result, the receiving taper-tube geometry for 180 mm inlet diameter was decided and is shown in table 3.1. Figure 3.4 shows the result of reflection inside the designed taper-tube, in which maximum reflection is 2 reflections inside this taper-tube.

Table 3.1: Designed Taper-tube Geometry

D_i	D_e	T_L	θ_T
180 mm	65 mm	160 mm	19.7°

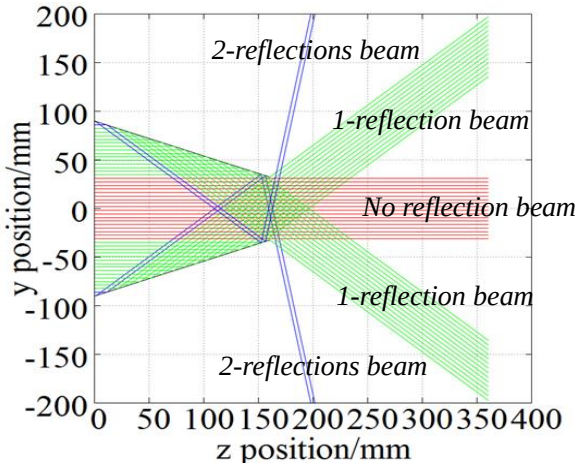

Figure 3.4: Designed Receiving Taper-tube.

There are (i) No reflection beam, (ii) 1-reflection beam, and (iii) 2-reflections beam.

3.1.4 Shape of Receiving Taper-tube

In this study, conical shape was chosen for the simplicity reason. Since the thruster of the current design of Microwave Rocket is circular tube, to be able to connect the taper-tube with the thruster conical shape is determined. Also, it was used earlier for the Microwave Rocket in [11]. Octagon taper-tube, however, was also selected as a candidate in this study, since the comparison of beam profile at the taper-tube exit due to different shape was also meant to be conducted. Sharp edges between the receiving taper-tube connection and the thruster is avoided, as plasma ignition at those edges might occurs in case of gyrotron is used. As a result, its shape is considered as the most convenient to connect with the thruster besides conical shape considering the above mentioned reasons.

Octagon taper-tube was designed as octagon inscribe circle. However, they

shared the same geometry except that the tapered angle was slightly difference due to the unattached surface between conical taper-tube wall and octagon taper-tube wall on the flat side. Figure 3.5 illustrates the difference, and resulting in 18.4°for tapered angle in case of octagon taper-tube.

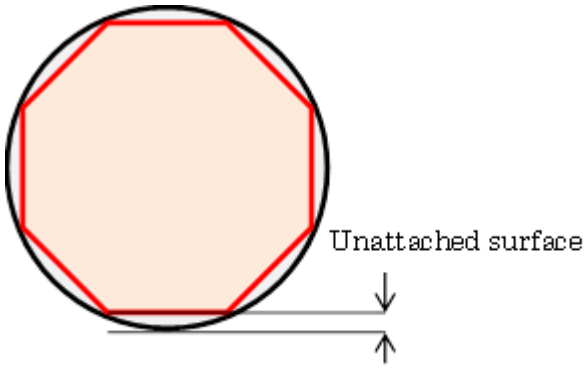

Figure 3.5: Cross section of conical (black) and octagon taper-tube (red). Due to unattached surface of octagon inscribe circle, it causes slightly different in tapered angle.

3.2 Experimental Setup and Measurement Apparatus

3.2.1 Receiving Taper-tube Setup

In a similar manner as explained in section 2.2.1, the experiment with receiving taper-tubes was conducted. Material been used is aluminum. The purposes of measurement were to determine transmission efficiency and to investigate the beam profile at taper-tube exit and compare with the simulation results.

Figure 3.6a illustrates the experimental setup schematic. Receiving taper-tube was located at the center of incident beam which its inlet was 220 mm from the

parabolic reflector. On the left, parabolic mirror reflects the transmitted wave from transmitter, and then passed through taper-tube. Receiver was put on the two dimensional stages (on the right). Both conical taper-tube and octagon taper-tube experiments were conducted the same way. Figure 3.6b shows the actual experimental setup with the deployment of high loss absorber.

3.2.2 Measurement Method

Vertical polarization

Similar to when the incident beam measurement was carried using the receiver on two dimensional moving stages, taper-tube was put and the measurement was conducted after the entire beam passed through taper-tube exit. Since at the exit of taper-tube concentrator, there are mainly 3 regions which are defined as (i) No reflection beam, (ii) 1-reflection beam, and (ii) 2 -reflections beam. Thus in this study the experiment were conducted as explain in the following.

Slot antenna at the receiver was located perfectly align with the beam direction (no tilt angle). Distances from conical taper-tube exit were 80 mm and 200 mm. At 80 mm distance, ray tracing simulation method showed that with two dimensional 200 mm on both x and y axis measurement surface moving translational perpendicular with the taper-tube exit plane, the receiver measured both none reflected beam and 1-reflection

beam. The stages moved 1 mm step in both *x* and *y* axis.

At distance 200 mm from the taper-tube exit, on the other hand, only none reflected beam enters the measurement surface. Moreover, in case of octagon taper-tube, since the tapered angle was slightly different, measuring distance was 85 mm and 230 mm instead to obtain the similar result. Figure 3.7 shows the measurement apparatus.

Horizontal polarization

In this experiment, the incident beam was reflected inside the taper-tube with some tapered angle depending on the taper-tube shape thus the direction of electromagnetic wave was altered. Figure 3.8 explains how the direction is changed. And at the receiver, slot antenna was used to receive the beam hence direction of the incoming wave has an effect on the measurement. Slot antenna has quite good directivity in its horizontal plane. Its vertical plane, however, cannot detect the signal and hence the receiver was changed in position as shown in figure 3.9. And then the experiment was conduct in all cases as explained earlier.

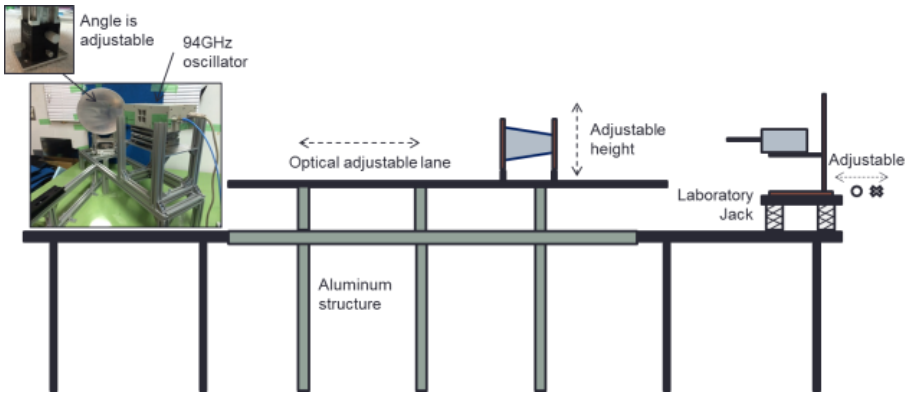

Figure 3.6a: Experimental setup schematic. 94GHz (left) transmitter transmitted the wave and is reflected at parabolic mirror attached with tilt stage. Receiving taper-tube was fixed along the lane which was the beam direction. Distance from mirror to taper-tube inlet was 220 mm.

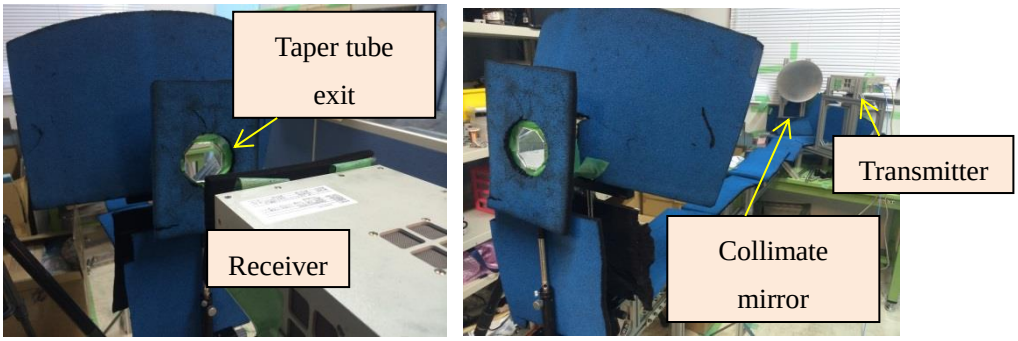

Figure 3.6b: Actual experimental setup.

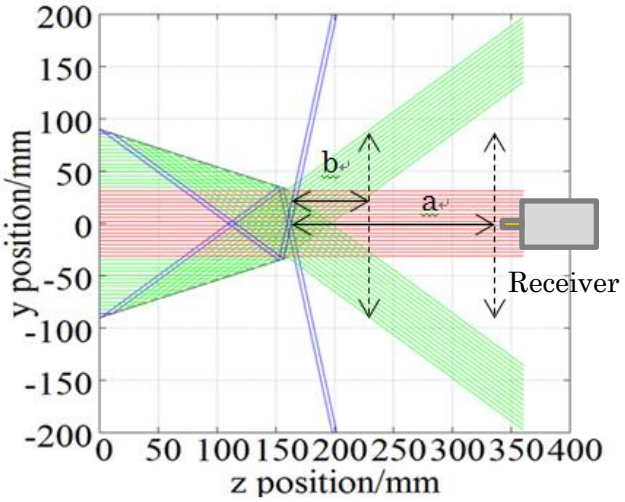

Figure 3.7: Measurement variables. (*a* and *b*) refers to distance from taper-tube exit to receiver which a = 200 mm for conical taper-tube while *a*= 230 mm for octagon. *b*, however was 80 and 85 mm for conical and octagon case respectively.

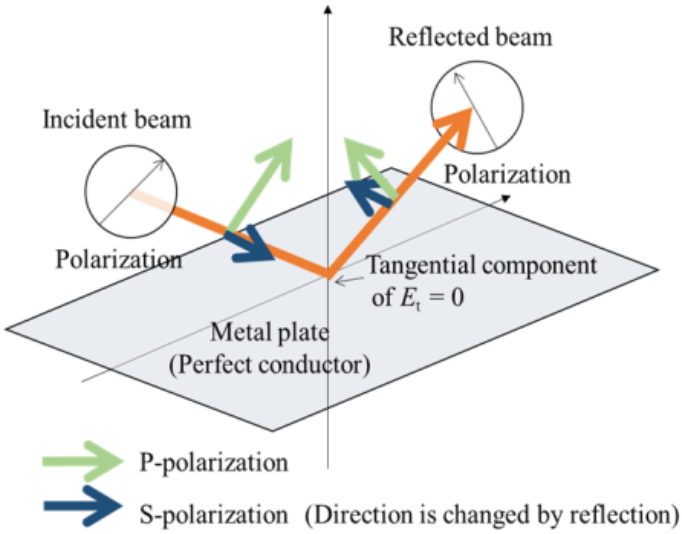

Figure 3.8: The direction of EM-wave that was altered due to the reflection with metal plate.

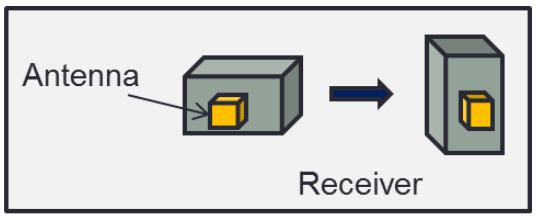

Figure 3.9: Changing in position of receiver. In order to measure horizontal polarization caused by the reflection of incident wave with the taper-tube wall.

1-reflection beam measurement

As explained in the previous section in this chapter, the design taper-tube produces 3 main regions at its exit, no reflection beam, 1-reflection beam, and 2-reflections beam. Nevertheless, number of reflections can exceed 2 depends on the parameter and variables yet in this study 2 times reflection inside the taper-tube was the maximum number.

Antenna was used to detect and measure the beam at taper-tube exit, however with the experimental setup as shown in figure 3.7 above the receiver and antenna was pointed perpendicular with the taper-tube exit. Even though 1-reflection beam was detected when b is equal to 80 mm and 85 mm in conical and octagon taper-tube case respectively, antenna had an angle equal to θ_{ref} with respect to the 1 reflection beam. So that antenna gain effect did exhibit in this case. Table 3.2 shows the angle of reflection for conical and octagon taper-tube.

In order to avoid antenna gain effect, receiver was set in a manner as shown in figure 3.10 instead. Receiver was fixed on the two dimensional stages as earlier but with the custom made aluminum rod fixer so that the angle was able to change freely. Figure 3.11 illustrates the actual experimental setup. The distance from taper-tube exit to the antenna at receiver was 80 mm and 85 mm for conical and octagon respectively. Experiment was done on both side of taper-tube exit.

Table 3.2: Angle of reflection (θ_{ref})

	Conical Taper-tube	Octagon Taper-tube
1 reflection beam	39.5°	36.7°
2 reflections beam	79.1°	73.5°

2-reflection beam measurement

The measurement was done in a similar manner as mentioned in previous measurement but with the angle of reflection equals to 79.1°and 73.5°for conical and

octagon taper-tube respectively. Distance between taper-tube exit and antenna was for conical taper-tube 14 mm and for octagon taper-tube 30 mm. Experiment was carried on both side (left and right) of the taper-tubes exit.

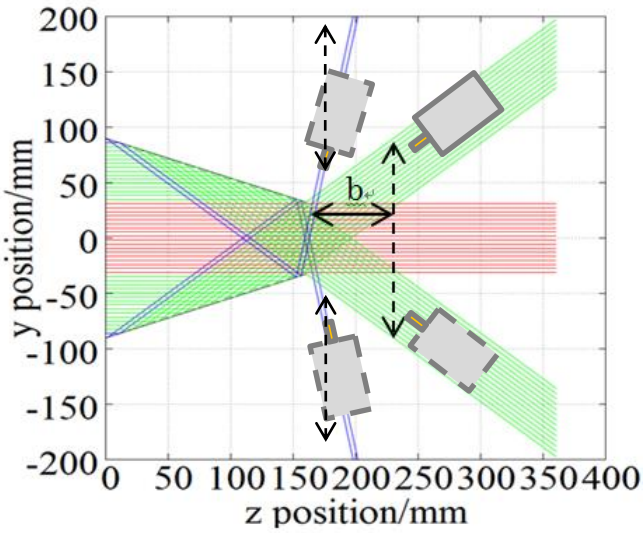

Figure 3.10: Experimental apparatus for 1 and 2 reflection beam (top view). The measurements were conducted on both side of the taper-tube exit. Angle of reflection was set and aligns with the receiver. Distance from taper-tube exit to receiver (*b*) was, for one-reflection measurement, 80 mm and 85 mm, and for two-reflection measurement 14.5 mm and 30mm for conical and octagon taper-tube respectively

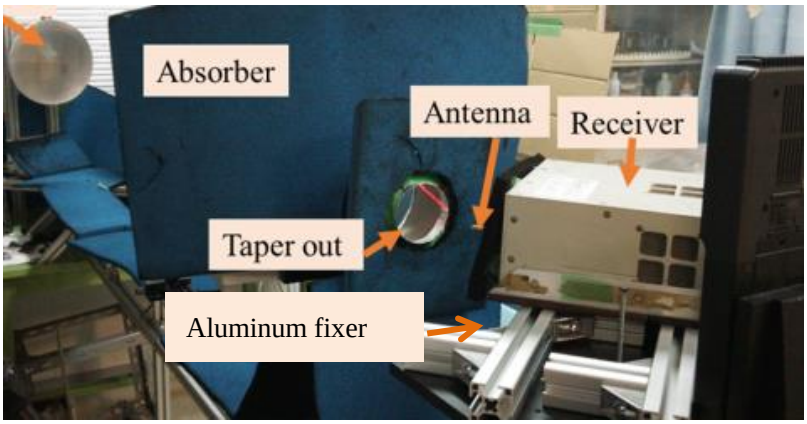

Figure 3.11: Actual experimental setup with receiver on the aluminum custom made fixer so that the angle was being able to change freely.

3.3 Experimental Result and Discussion

In this section, experimental results are separated into (1) Vertical and Horizontal polarization around center of the taper-tube (expected no tilt angle between antenna and taper-tube exit plane), and (2) reflection beam measurements in which both are separately shown for conical and octagon taper-tube.

Figure 3.12 shows the conical and octagon taper-tube experiment with experimental setup as shown in figure 3.7 at distance 80 mm and 85 mm depending on taper-tube shape from taper-tube exit to receiver. Meanwhile, figure 3.13 shows their cross sectional at centered plane in both x and y axis.

At distance 200 mm from taper-tube exit to receiver (conical taper-tube) and 230 mm (octagon taper-tube), results are shown in figure 3.14. Note that in every case, taper-tube exit is located at the center (x and y = 0). And it has diameter of 65 mm. Thus, the results shown in between -3.25 $\leq x$ and y position $\leq$ 3.25 were expected being no reflection beam otherwise one reflection beam. The x and y axis represent the location along the measurement surface (200 mm x 200 mm). And scale on the right hand side is in μW. Illustration of 1 and 2-reflection beam measurement results, they are shown in figure 3.15 which are in accordance with the experimental setup shown in figure 3.10 in the previous section.

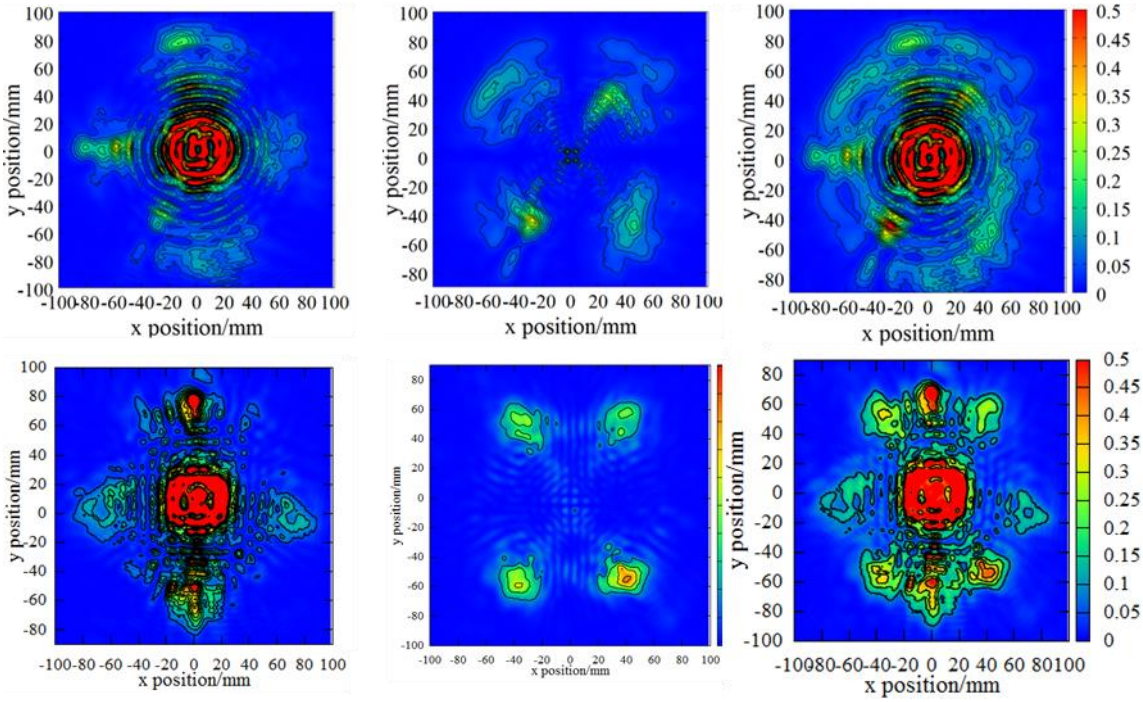

Figure 3.12: Power density experimental result. Upper row shows conical taper-tube experimental result while another shows results for octagon case. Distance from tapered exit were 80 mm and 85 mm for conical and octagon taper-tube respectively. From left to right, first column is the power density of vertical polarization, second column is the power density of horizontal polarization and third column is the summation of result in both first and second column for each case (conical and octagon taper-tube. Horizontal and vertical axis shows position in *x* and *y* direction with centered at 0. Scale on the most right shows the intensity of power density in μW.

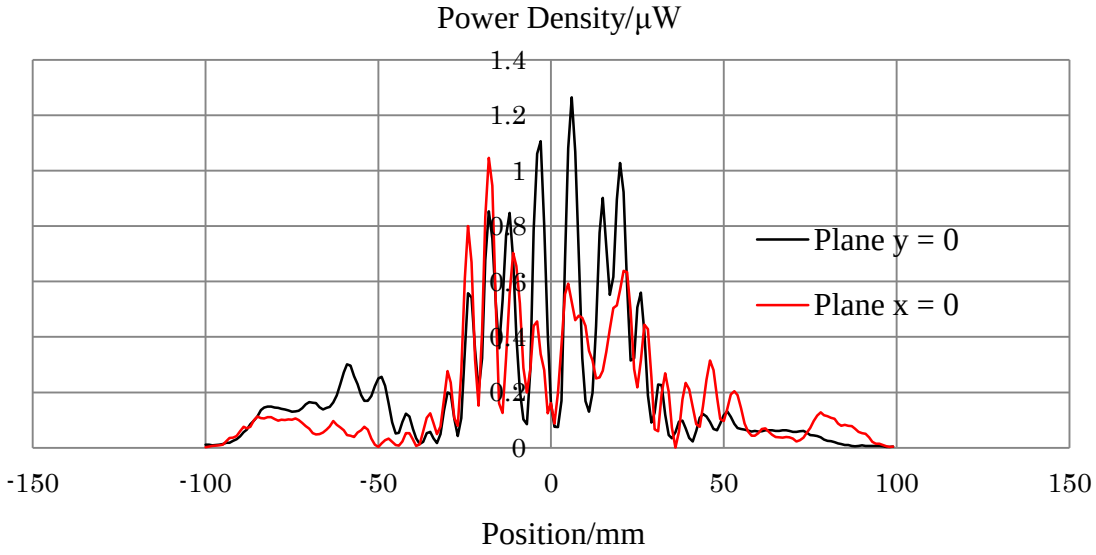

Figure 3.13a: Power density at plane x and y =0 for conical taper-tube (vertical polarization). Distance from taper-tube exit to the receiver was 80 mm. *X* and *Y* axis represent position along the planes and power density in μW respectively

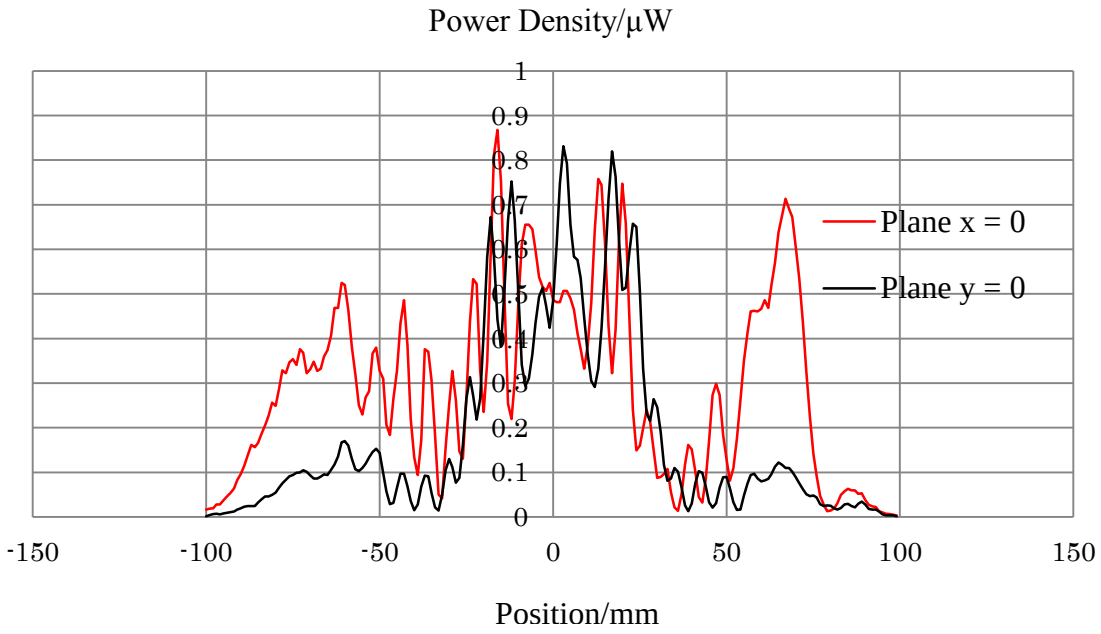

Figure 3.13b: Power density at plane *x* and *y* =0 for octagon taper-tube (vertical polarization). Distance from taper-tube exit to the receiver was 85 mm. *X* and *Y* axis represent position along the planes and power density in μW respectively

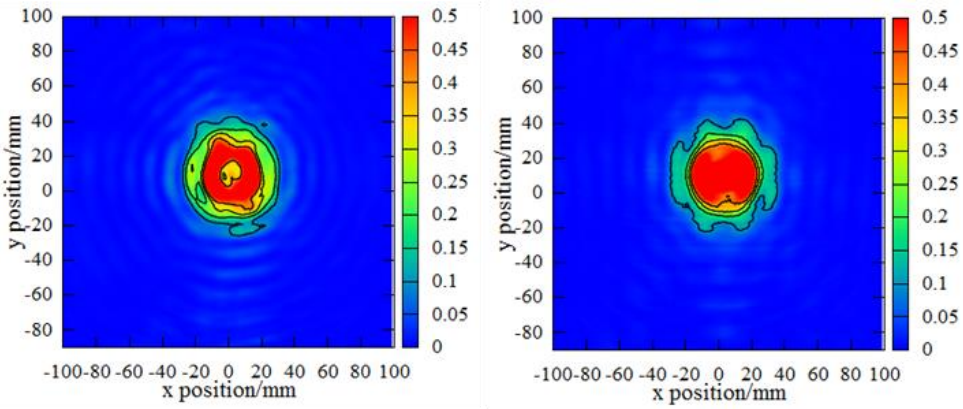

Figure 3.14: Power density experimental result at distance 200 mm and 230 mm from conical and octagon taper-tube exit to the receiver respectively (vertical polarization). Horizontal and vertical axis shows position in *x* and *y* direction with centered at 0. Scale on the most right shows the intensity of power density in μW.

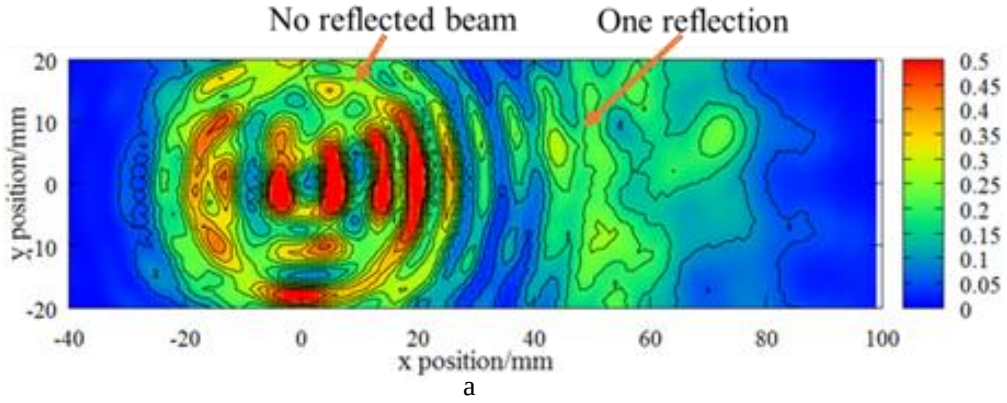

a

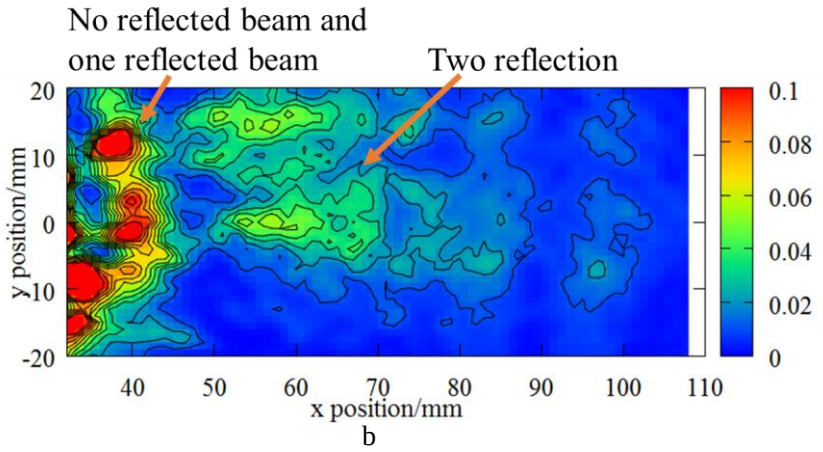

b

Figure 3.15: Illustration of (a) one and (b) two reflection beam results. Both are conical taper-tube case at 80 mm and 14.5 mm as distance from taper-tube exit to receiver.

From the experimental results shown above, figure 3.12, at 80 mm and 85 mm from the taper-tube exit there were both no reflection beam and 1 reflection beam. Power density around the center of the measurement surface that stays within ± 3.25 mm for both x and y axis was assumed as no reflection beam, while the other are 1 reflection beam. Cross section was done in order to show the profile in details. Power density in both taper-tubes exceeded the peak power density of incident beam which was approximately around 0.5μW. In a meanwhile, figure 3.14 shows that if receiver were moved further at (conical) 200 mm and (octagon) 230 mm, only no reflection

beam was measured. Since one and two reflection both leave taper-tube exit with angle of reflection and they did not enter the measurement surface at these conditions. On the other hand, one and two reflections beam were measured by changing the angle of receiver with respect to the angle of reflection of the beam, and parts of the results are illustrated in figure 3.15.

As a result, the power fraction of each beam was integrated and estimated separately. Cylindrical integration was used to estimate one and two reflection beam for conical case and the Eq.3.2 shows the integration been used in which *P* is estimated power fraction, *S* is power density at each point, and r is the radius from the center of taper-tube exit. For one and two reflection beam of octagon taper-tube, it was estimated using approximation method, trapezoidal rule, similarly with no reflection beam. Table 3.3 shows the result of integration. η_{trans} that is shown in table 3.3 represent transmission efficiency in percentage which was calculated using Eq.3.3

$$P = 2\pi \int rSdr \qquad 3.2$$

$$\eta_{\text{trans}} = \frac{\text{Power fraction } (P)}{\text{Total Power of incident beam}} \; x\; 100 \qquad 3.3$$

Table 3.3 shows the estimation of power fraction of each beam where standard deviation was calculated.

Table 3.3: Experimental result on power fraction

Power Fraction	Conical	Octagon
No Reflection Beam/mW	1.13 ±0.1	1.11±0.15
1-Reflection Beam/mW	1.94 ±0.4	1.77±0.18
2-Reflection Beam/mW	0.095 ±0.05	0.11±0.014
Total/mW	3.17±0.87	2.99±0.34
Incident beam/mW	3.63	

In both cases, errors came from propagated error from the measured voltage. Both taper-tube results show the good transmission efficiency as it almost achieved incident beam total power even though with error taken into account.

3.4 Comparison of experimental and simulation results

The comparison between the experimental results of power fraction is compared with the simulation result using ray tracing. Figure 3.16 and 3.17 shows the comparison at distance 80 mm and 85 mm from taper-tube exit to the receiver for conical and octagon taper-tube respectively.

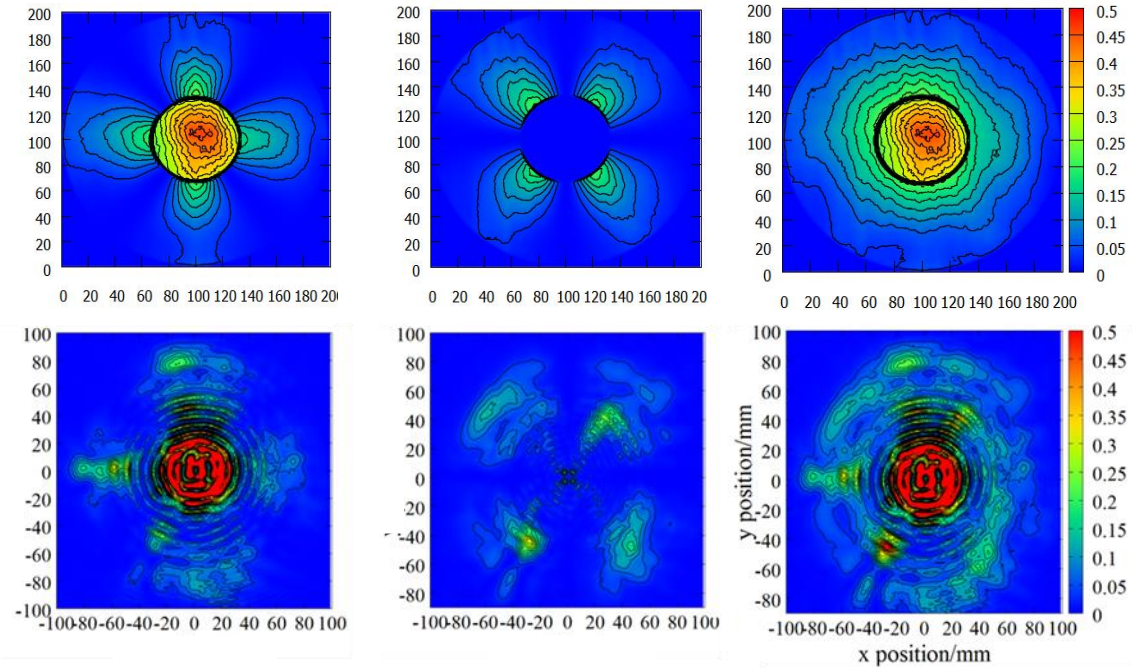

Figure 3.16: Conical taper-tube beam profile comparison. From left to right, vertical polarization, horizontal polarization, and the summation. First row shows computational result from ray tracing while 2nd row shows experimental result.

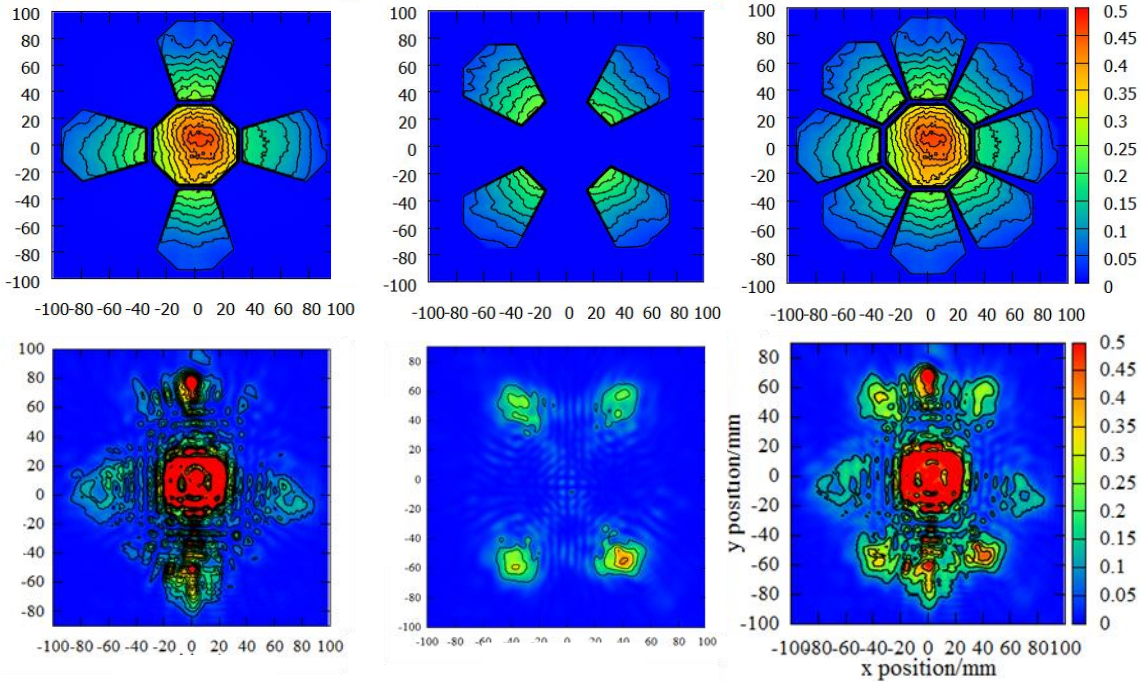

Figure 3.17: Octagon taper-tube beam profile comparison. From left to right, vertical polarization, horizontal polarization, and the summation. First row shows computational result from ray tracing while 2nd row shows experimental result.

From the comparison, it shows that by using ray tracing method it could qualitatively reproduce the beam profile at taper-tube exit with the same incident beam profile. The simulation was calculated, using the experimental incident beam profile, and concerning the direction of polarization but neglecting other wave effects. Power fraction comparison was made and shown in table 3.4 and 3.5.

In the simulation incident beam was spilled out of taper-tube inlet, part of it did not enter the taper-tube due to that incident beam was not an exact Gaussian profile. Thus, not the entire incident beam with total power of 3.63 mW entered the taper-tube but 3.44 mW and 3.35 mW for conical and octagon taper-tube respectively. The result shown in table 3.4 shows that the trend of power fraction of no reflection beam, 1-reflection beam, and 2-reflections beam shows some agreement between experimental and simulation results except 2-reflection beam power fraction. Also results show that both conical and octagonal taper-tube achieve high transmission efficiency, 92% and 86% respectively.

Table 3.4 Comparison between experimental and simulation power fraction for conical taper-tube

Power Fraction	Experiment	Simulation
No reflection beam/mW	1.13 ±0.1 (32.8 ±2.9%)	1.17 (34.0%)
1-reflection beam/mW	1.94 ±0.4 (56.4 ±11.6%)	2.12 (61.6%)
2-reflection beam/mW	0.095 ±0.05 (2.8 ±1.4%)	0.15 (4.4%)
Total/mW	3.17±0.87 (92.0±15.9 %)	3.44 (100%)

Table 3.5 Comparison between experimental and simulation power fraction for octagon taper-tube

Power Fraction	Experiment	Simulation
No reflection beam/mW	1.11±0.15 (32.3 ± 4.4%)	1.07 (31.9%)
1-reflection beam/mW	1.77±0.18(60.88 ± 5.3%)	2.07 (61.8%)
2-reflection beam/mW	0.11±0.014(10.74 ± 0.5%)	0.21 (6.3%)
Total/mW	2.99±0.34(86.9±9.8%)	3.35 (100%)

3.5 Conclusion

Ray tracing method was used to design the taper-tube concentrator in which backward reflection to the incident beam direction is to be avoided. Since the size of taper-tube is much larger than the wavelength transmitted from 94GHz transmitter thus ray tracing was chosen due to its simplicity and low computational cost.

Experiment was conducted to investigate the beam profile at taper-tube exit. The transmitter transmitted the millimeter wave passed through taper-tube and the receiver was used to measure the wave on the exit size. The measurement was carried to measure no reflection beam, 1-reflection beam, and 2-reflections beam according to the prediction from ray tracing simulation result.

Experimental results show that the wave at the exit behaves similar as predicted. By comparing to the result from ray tracing method, it is clearly that ray tracing is able to quantitatively reproduce the wave at taper-tube exit.

Quantitatively comparison shows that there were no reflection beam, 1-reflection beam, and 2 reflections beam. Power fraction of each beam was estimated, and it shows some agreement with the simulation result. Also the transmission efficiency of both taper-tubes achieved high value, 92 and 86 percent. Moreover, the trend of each beam output also shows good agreement with the simulation results.

In a nutshell, taper-tube concentrator is expected to deliver most of the entire incident beam throughout its exit in which thruster is connected with in case of Microwave Rocket. And ray tracing simulation method is able to reproduce the phenomenon inside the taper-tube as its results show consistency with experimental results.

Chapter 4: Taper-tube for Microwave Rocket

4.1 Microwave Rocket's taper-tube concentrator design

Beam receiving taper-tubes concentrator for Microwave Rocket experiment was conducted using gyrotron as beam source. Table 4.1 shows conical and octagon taper-tube concentrator geometry. Inlet diameter was fixed due to the incident beam diameter (240 mm) from the beam transmission system while exit diameter was fixed according to the thruster size. Hence, length and tapered angle was decided using ray tracing method as explained in the previous chapter.

Shape, however not the only difference between these 2 taper-tubes but also the type of material used. Aluminum was chosen due to its strength, low cost, and easy to be found. Thus, conical taper-tube was manufactured using aluminum sheet with thickness of 1 mm, it was fabricated in 2011 prior to this study.

On the other hand, in an attempt to reduce the weight of taper-tube concentrator, aluminum mesh sheet was used instead to fabricate octagon taper-tube. Since in case flight demonstration was to be conducted, by using aluminum mesh instead of metal sheet it was expected that total weight of Microwave Rocket would be reduced in a significant amount. In this study, aluminum mesh sheet assembling with 8 carbon fiber

rods were used to fabricate the octagon shape of taper-tube in order to withstand the thruster weight. Conical taper-tube is able to directly connect with the thruster due to the same cross sectional shape, while octagon taper-tube needs an aluminum connector.

Table 4.1 Taper-tube geometry. (for Microwave Rocket)

Inlet Diameter	Exit Diameter	Length
250 mm	56 mm	470 mm

As a result, conical taper-tube concentrator was weight approximately around 700g. In contrast, by using aluminum mesh sheet as in octagon taper-tube it weighted approximately 260g. And since size of mesh, was specified as 0.1mm which is very much smaller compare to wavelength of millimeter wave beam produced by gyrotron. Gyrotron transmits 170GHz millimeter wave beam which is equal to around 1.7 mm wavelength hence, the use of aluminum mesh sheet as taper-tube wall was expected to show no difference with using aluminum sheet as in conical taper-tube. Figure 4.1 shows both receiving taper-tubes.

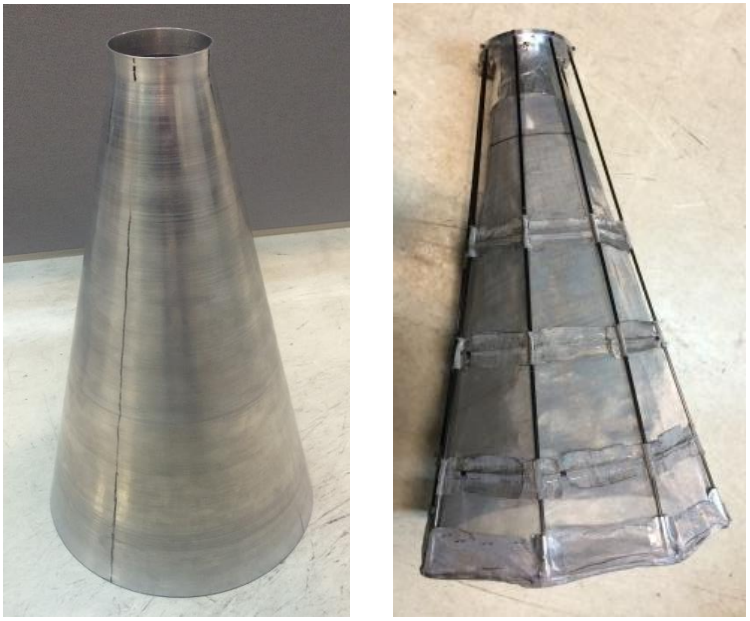

Figure 4.1: Taper-tube concentrator for Microwave Rocket. Left: Conical taper-tube using aluminum metal sheet. Right: Octagon taper-tube using aluminum mesh sheet.

4.2 Aluminum metal sheet and aluminum mesh sheet

Prior to the Microwave Rocket experiment, the measurement of beam power profile and power fraction was carried for the comparison in the same manner as explained in chapter 3 using 94GHz transmitter. The experiment was conducted as shown in figure 3.7 in chapter 3 only and also only conical taper-tube was done. Figure 4.2 shows the conical taper-tube both in aluminum meatal and mesh.

Distance from taper-tube exit was 60mm, 155mm, and 320 mm as calculated from ray tracing method in order to observe no reflection, 1 reflection and 2-reflections beam. Figure 4.3 illustrates the experimental result at distance 155 mm while table 4.2 shows the power fraction estimation. Note that this power fraction of 1 and 2-reflections beam exhibit antenna gain effect as receiver was fixed at only one position thus they

don’t represent the actual power fraction. The experiment was carried on the purpose of comparison only.

It is suggesting that using mesh sheet as taper-tube concentrator wall it delivered almost the same result as metal sheet in tern of power fraction. Beam profile, on the other hand, using metal sheet clearer profile was obtained. Due to the fluctuation and non-flat characteristic of aluminum mesh sheet, the reflection beam was not clearly seen. Estimation is shown in table 4.2.

As a result, the reflection phenomena inside the taper-tube was expected to be similar in both case but the angle of reflection and the direction where the beam is reflected was not well align in case of mesh sheet was used.

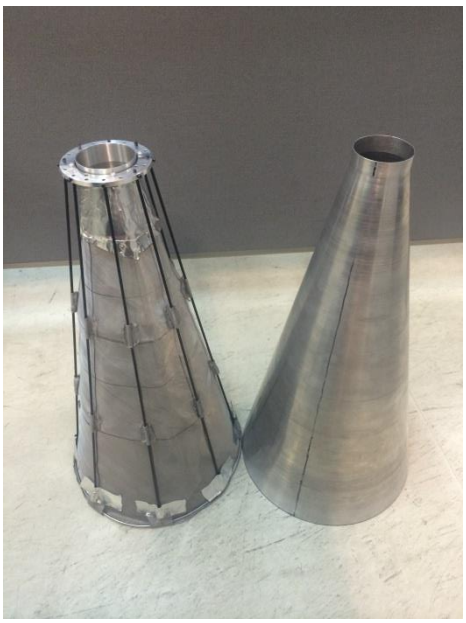

Figure 4.2: Conical taper-tube. Left: aluminum mesh. Right:aluminum metal.

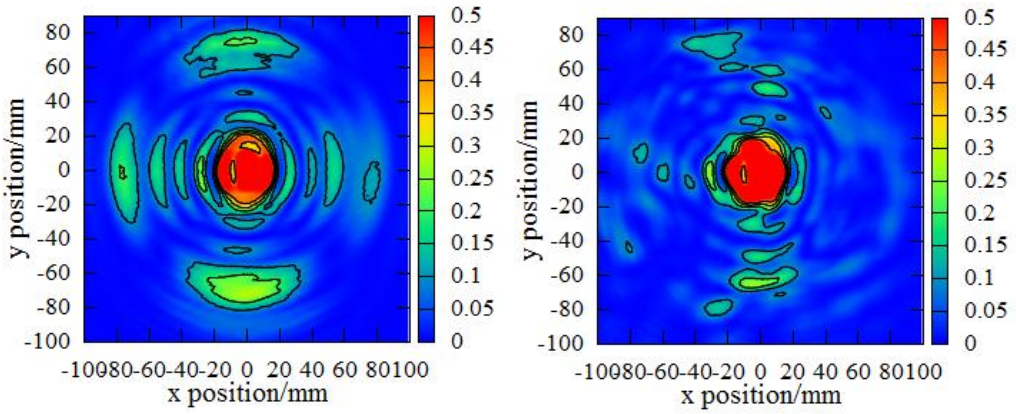

Figure 4.3: Experimental result on beam power profile. Left: Aluminum metal sheet. Right: Aluminum mesh sheet.

Table 4.2: Power fraction comparison of conical metal and mesh sheet taper-tube

	Metal Sheet	Mesh Sheet
No reflection/mW	1.14	1.17
1-reflection/mW	1.28	0.95
2-reflection/mW	0.25	0.22
Total/mW	2.67	2.34

4.3 Experimental Setup and Measurement Apparatus

The measurement of Microwave Rocket's thrust performance was conducted earlier in 2012, using conical taper-tube [11]. The transmission mirror system, a part of the development prior to the experiment in this study [18], which expanded 40.8 mm beam diameter from the corrugated waveguide connected with gyrotron to 240 mm in order to suppress the divergence angle and attempt to collimate the millimeter wave beam. In this study, on the other hand, in a similar manner as in [11], octagon receiving

taper-tube using aluminum mesh was used in the experiment having gyrotron as a beam source. Experimental schematic is shown in figure 4.4.

4.3.1 Microwave Rocket's thrust-stand

Gyrotron was connected with corrugated waveguide and transmitted high power millimeter wave beam. Beam was ejected at the output with Gaussian profile, and reflected the transmission mirror system. Beam was expanded from 40.8 mm to 240 mm at. Current designed of Microwave Rocket comprised of taper-tube concentrator and thruster, was stability hung on thrust-stand coupling with aluminum wire and pulleys system. Thrust-stand itself was able to be put on the ground without any additional support. Thruster and taper-tube were stabilized by aluminum wires and pulleys. Thruster was connected with taper-tube concentrator with nuts and bolts at the outer part. Figure in the right hand side of figure 4.4 shows the actual experimental setup.

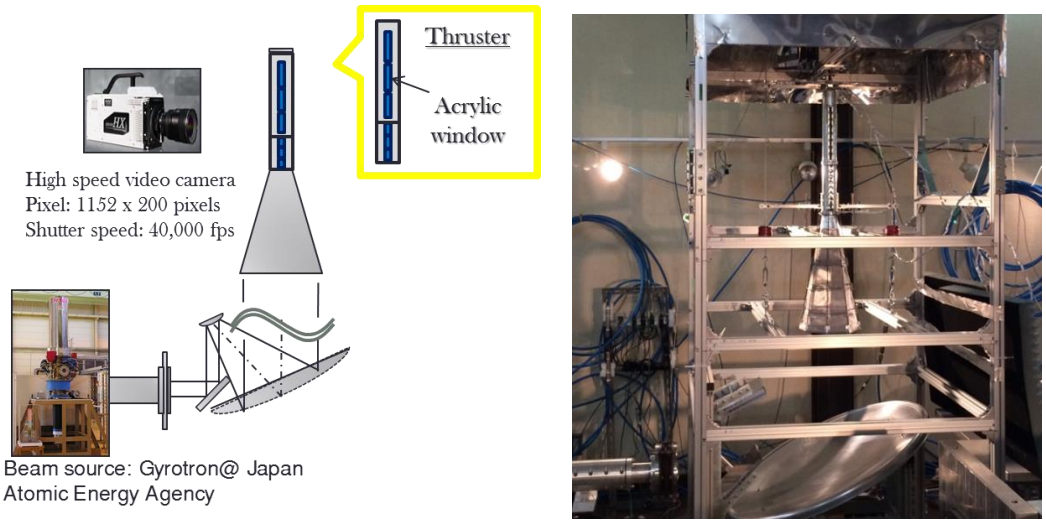

Figure 4.4: Experimental setup at JAEA. Left is the experimental schematic. Right figure is the actual setup. Gyrotron transmitted 170GHz MMW through corrugated wave guide and reflected the transmission mirror system before enter the taper-tube. High speed video camera with shutter speed of 40,000 fps was employed to capture the plasma inside the thruster through the attached acrylic window.

4.3.2 Thruster and measurement system

Pressure sensors were equipped at the top of the thruster (closed-end) and at the half of the length of the thruster. These pressure sensors were used to investigate pressure inside the thruster and account for the moment millimeter wave hit the thruster reflector (at the top) and blasting wave was then created. Thruster was an aluminum tube with parabolic reflector at the closed-end which used to focus the incoming wave and create breakdown in the air into plasma. This parabolic reflector was so called collector.

In addition, acrylic window was also integrated on the side wall of the thruster in which it is used to observed plasma's ionization front propagation inside the thruster. High speed video camera was used to capture the frames to observe plasma inside the

thruster through the acrylic window.

4.4 Experimental Results and Discussion

4.4.1 Plasma Ignition

Gyrotron transmitted millimeter wave beam to Microwave Rocket as explained earlier. The thruster was fixed standstill so that it did not move while the high speed camera was capturing the phenomenon inside the thruster. Figure 4.5 shows the plasma inside the thruster that was captured by high speed video camera. Experimental results show that there was certainly plasma ignition inside the thruster caused by the focusing beam collector. Plasma then expanded and glowed into incident beam direction as well as the ionization front was propagated in the same direction.

Gyrotron transmitted millimeter wave beam with different power compare to the experiment that conducted in 2012 using conical receiving taper-tube. In the previous experiment, it transmitted power at 638 kW while this time it transmitted 561 kW. Even though the transmitted power is lower, octagon taper-tube succeeded in conveying sufficient power to the collector inside the thruster as plasma and ionization front propagation could be observed.

Figure 4.5: Experimental result. Plasma was ignited in the air and glowing inside the thruster to the incident beam direction. Time scale in ms.

4.4.2 Ionization Front Propagation Velocity

As it can be seen from figure 4.3 that plasma and ionization front were glowing and propagating towards the beam direction (opened-end), by using high speed video camera the velocity is simply analyzed from very small time difference and the position of the ionization front. As a result, ionization front propagation velocity inside the thruster in case of using octagon taper-tube was approximately 170 m/s while in 2012, Microwave Rocket with conical taper-tube, the ionization front propagation velocity was estimated around 560 m/s.

4.4.3 Peak Power Density and Thrust Performance

Oda et al., [19] shows the empirical relation between the ionization front propagation velocity and peak power density as it is shown here in Eq.4.1. This equation was obtained from figure 4.6. As a result, using equation 4.1 with the result obtained in this study along with the previous conical taper-tube result the comparison

is shown in figure 4.7.

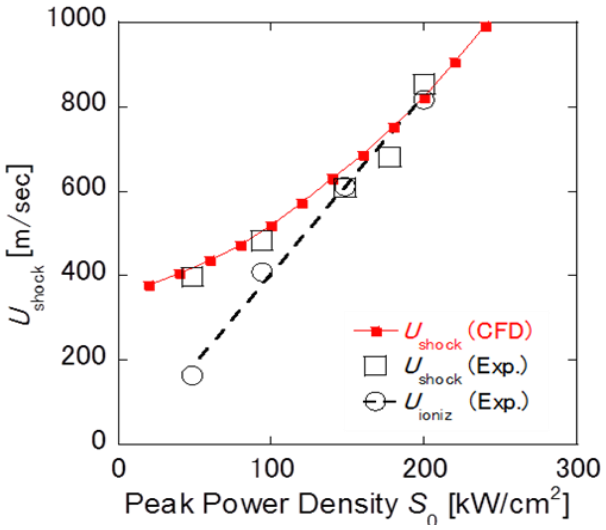

Oda et al.,2009

Figure 4.6: Relation of Ionization front propagation velocity and peak power density.

$$U_{ionization} = 4.19S_0 - 14.9 \quad (4.1)$$

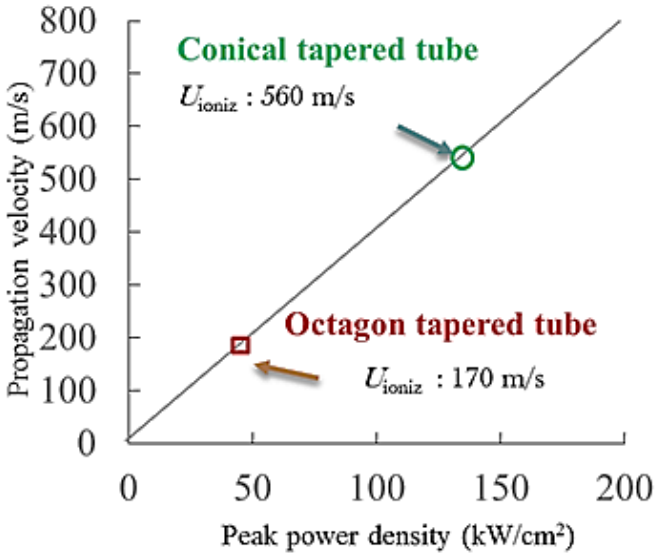

Figure 4.7: Comparison of experimental results of ionization front propagation velocity for conical and octagon taper-tube.

Experimental result suggests that with such low velocity of ionization front propagation in octagon case, subsonic velocity, thrust generation is insufficiently. As

Microwave Rocket denotes the detonation cycle to create thrust, with subsonic velocity it was difficult to generate high thrust. Impulsive thrust was deduced from pressure histories. Nonetheless, in case of conical taper-tube thrust impulse was only 71mNs/pulse. The ionization front propagation velocity was too high and it also did not contribute to thrust generation sufficiently.

As a consequence, the optimization of taper-tube concentrator must be done and thus the ionization front velocity in between octagon and conical taper-tube should be achieved. As well as the power density inside the thruster the beam passes through taper-tube should be investigated.

4.5 Conclusion

Experiment was carried using octagon taper-tube with aluminum mesh sheet connected with thruster. Taper-tube geometry was determined using ray tracing and it was fabricated in order to reduce its weight aluminum mesh was used. High speed camera was used to capture the moment of ignition of plasma from atmospheric air breakdown phenomena, and also the ionization front propagation inside the thruster. Since thruster was attached with acrylic window, it is able to observe the propagation of ionization front through that window.

Comparison between aluminum metal and mesh conical taper-tube was made.

The power fraction shows the some agreement while qualitatively the beam profile of conical taper-tube using metal sheet was observed clearer.

Experimental result, using gyrotron, shows that plasma was observed inside the thruster which means that octagon taper-tube succeed in deliver the incident beam into the thruster. And also ionization front propagation was estimated at around 170 m/s. In the previous study it was approximately 560 m/s when conical taper-tube was used. Nonetheless, either of taper-tube thrust estimation shows that thrust to weight ratio is less than 1 thus flight demonstration cannot be achieved.

Chapter 5: Conclusion

1. 94 GHz transmitter with horn antenna was used as millimeter wave source. It transmitted millimeter wave beam to the collimate mirror which created parallel beam. Resulting in incident beam with beam diameter around 150 mm.
2. The experiment on taper-tube concentrator for millimeter wave was carried. Its geometry was determined using ray tracing method. Receiver was used to measure the beam that leaves taper-tube. As a result, there are no reflection beam, one reflection, and two reflections beam. Power fraction of each beam was also estimated as well as transmission efficiency. 92% and 86% were achieved for conical and octagonal taper-tube respectively.
3. The comparison between experimental and simulation result was made and it shows good agreements both qualitatively and quantitatively. The power fraction comparison shows that the ray tracing simulation could reproduce the millimeter wave experiment.
4. Taper-tube concentrator for Microwave Rocket experiment using 170GHz gyrotron as beam source was conducted. Result shows that plasma was ignited and glowed inside the thruster. Ionization front propagation velocity was observed and measured, approximately 170 m/s. Maximum thrust was 2.7 N.

Reference

[1] A. Kantrowaitz, “Propulsion to Orbit by Ground-Based Lasers,” Astronautics and Aeronautics, , 1972 .

[2] L. N. Myrabo, “World record flights of beamed-riding rocket light craft,”American Institute of Aeronautics and Astronautics Paper N, pp. 2001-3798,, 2001

[3] K. Sakamoto, A. Kasugai, K. Takahashi, R. Minami, N. Kobayashi, and K. Kajiwara. Achievement of robust high-efficiency 1mw oscillation in the hard-self-exitation region by a 170ghz continuous-wave gyrotron. Nature Physics, 3(6):411–414, 2007.

[4] J.P. Knecht and M.M. Micci. Analysis of a microwave-heated planar propagationg hydrogen plasma. AIAA Journal, 26(2):188{194, 1988.

[5] K.L.G. Parkin and F.E.C. Culick. Feasibility and performance of the microwave thermal rocket launcher. In Kimiya Komurasaki, editor, Beamed Energy Propulsion: Second International Symposium on Beamed Energy Propulsion, pages 407{417. American Institute of Physics, 2003.

[6] K.L.G. Parkin, L.D.DiDomenico, and F.E.C. Culick. The microwave thermal thruster concept. In Kimiya Komurasaki, editor, Beamed Energy Propulsion: Second International Symposium on Beamed Energy Propulsion, pages 418{429. American Institute of Physics, 2003.

[7]Tatsuo Nakagawa, YorichikaMihara, Kimiya Komurasaki, Kouji Takahashi, Keishi Sakamoto, Tsuyoshi Imai, “Propulsive Impulse Measurement of a Microwave-Boosted Vehicle in the Atmosphere”,Journal of Spacecraft and Rockets, Vol. 41, No. 1, pp.151-153, 2004.

[8] Y. Oda, T. Shibata, K. Komurasaki, K. Takahashi, A. Kasugai, and K. Sakamoto, “Thrust Performance of a Microwave Rocket Under Repetitive-Pulse Operation”, *J. Propulsion and Power* Vol. 25, No.1, pp118-122 (2009)

[9] T. P. G. Bussing, “An Introduction to Pulse Detonation Engines,” AIAA Paper, 94-0263, 1994

[10] M. Thumm. Progress in gyrotron development. Fusion Engineering and Design, 66:69{90, 2003.

[11] Masafumi Fukunari, Toshikazu Yamaguchi, Shohei Saitoh, Kenta Asai, Satoshi Kurita, Kimiya Komurasaki, Yasuhisa Oda, Ken Kajiwara, Koji Takahashi and Keishi Sakamoto “Thrust Performance and Plasma Generation of Microwave Rocket with Microwave Beam Space Transmission System” PPPS 2013

[12] Toshikazu Yamaguchi, Reiji Komatsu, Masafumi Fukunari, Kimiya Komurasaki, Yasuhisa Oda, Ken Kajiwara, Koji Takahashi, and Keishi Sakamoto “Millimeter-wave Driven Shock Wave for a Pulsed Detonation Microwave Rocket,” AIP Conf. Proc. 1402, 478, 2011

[13] Ya-Lun Tsai, Mount-Learn Wu, Hsiao-Chin Lan, and Jenq-Yang Chang, “Design of Low-Loss Tapered Waveguide by Applying Photonic-Crystal-Based Microlens in Telescopic Structure”-OSJ, 2006

[14] Stephen G. Larew, Timothy A. Thomas, Mark Cudak, Amitava Ghosh, “Air Interface Design and Ray Tracing Study for 5G Millimeter Wave Communications”, IEEE, Globecom 2013 Workshop - Emerging Technologies for LTE-Advanced and Beyond-4G

[15] Sebastian Priebe, Martin Jacob, Thomas Kurner, “Calibrated Broadband Ray Tracing for the Simulation of Wave Propagation in mm and Sub-mm Wave Indoor Communication Channels”, IEEE, European Wireless 2012

[16] Paul-Henri Tichit, Shah Nawaz Burokur, and André de Lustrac, “Waveguide taper engineering using coordinate transformation technology”, Optics Express, Vol. 18, Issue 2, pp. 767-772 (2010)

[17] Hans-Georg Unger “Circular Waveguide Taper of Improved Design” Bell System Technical Journal Volume 37, Issue 4, pages 899–912, July 1958

[18] Toshikazu Yamaguchi, Kimiya Komurasaki, Yasuhisa Oda, Ken Kajiwara, Koji Takahashi, and Keishi Sakamoto, “Millimeter-wave Beam Conversion with Quasi-optical Mirrors for Microwave Rocket Launch Demonstration”, BEAMED ENERGY PROPULSION: Seventh International Symposium, AIP Conf. Proc. 1402, pp. 467-477

[19] Yasuhisa Oda, Kimiya Komurasaki, Koji Takahashi, Atsushi Kasugai, and Keishi Sakamoto, “Plasma Generation using high-power millimeter-wave beam and its application for thrust generation”, Journal of Applied Physics 100, 113307, 2006

[20] Toshikazu Yamaguchi, Reiji Komatsu, Kimiya Komurasaki, Yasuhisa Oda, Ken Kajiwara, Koji Takahashi and Keishi Sakamoto, “Interaction between Shock Wave and Plasma Region Ionized by Millimeter Wave Beam and Its Application to Pulse Detonation System as a Microwave Rocket”, IEEE, 2011

Conference

[1] Nat Wongsuryrat, Kenta Asai, Masafumi Fukunari, Toshikazu Yamaguchi and Kimiya Komurasaki “Design of Microwave Rocket Beamed Energy Propulsion Transmission Receiving System”, 宇宙輸送シンポジウム 2014